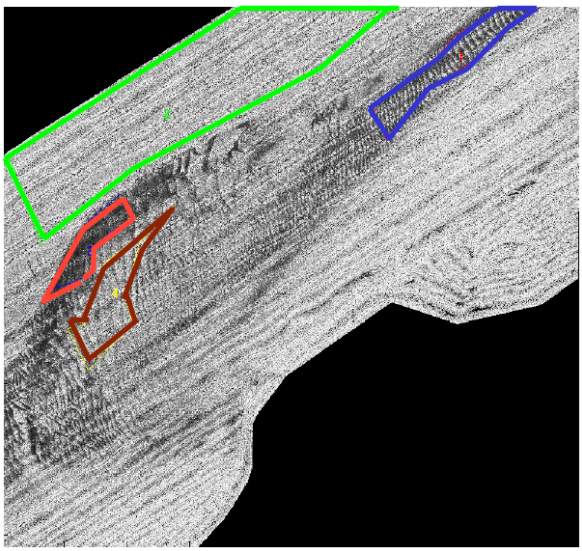

The study of SONAR images intelligent segmentation techniques

Research rapport in the framework of the grant CNCSIS ID_930

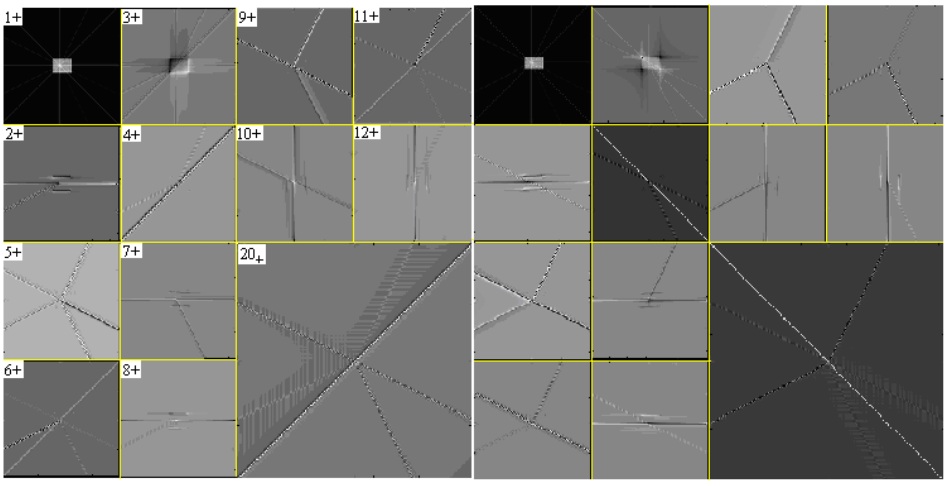

Corina Naforniţă, Ioana Firoiu, Cristina Stolojescu, Ioan Naforniţă, Sorin Moga, Alexandru Isar

Contents

1. Introduction

The first researches in the field of AI were made in our team 25 years ago. Professor Nafornita delivered a course and worked for the Romanian Army Research Institute. Later, our team had collaborations with the Tamasz Roska's research team regarding the Cellular NN, finalized by th PhD thesis[1].

In the year 2000 was presented the PhD thesis [2]. Finally, in the year 2003 was presented the PhD thesis [3]. We must mention that all the three doctors are former students from our faculty. After, Moga Sorin becomes assistant professor at ENST-Bretagne from Brest, France and he is now in a department of AI, giving a course of aid for decisions making and is the organizer of a master about the man-machine interaction. He was recently nominated honorary consul of Romania in Brest. We have already claimed that the NN of the cortex must be interpreted like a distributed memory of sequences. The temporal character of these patterns and their role in caring information permit us to see the NN like systems treating signals. All the members of our research team are specialized or intent to become specialists in signal processing. A very modern category of signal processing is the intelligent signal processing. There is, also, a great demand of aid for decisions making. The medicine doctors have a great need of assistance for the correct diagnosis of diseases, the geologists need correct information about the regions that they research and the communication engineers request more aid for making decisions concerning their communication networks. The applications of the aid for decisions making that we want to study in the framework of this grant are: the cardiac illness diagnosis, the underground undersea composition identification and the WiMAX networks radio-planning. The block diagram of an acquisition system dedicated to the aid for decisions making is composed by the acquisition system itself, followed by a denoising block, by a segmentation block and by a classification block. Usually the wavelets are used for denoising. One of the most difficult operations in SP is segmentation. This can be done using statistical methods or intelligent SP methods. Finally the classification can be done using statistical methods or NN. The previous achievements of our research team in the diagnosis of cardiac illness are the article [4] and the diploma project [5]. The subject of the article is the detection of the P wave. Its form and duration give valuable information about some cardiac illness. The article was presented at the best SP conference, ICASSP and represents the result of a visit during 6 months made by one of our colleagues at ENST-B, where his research was advised by Professor Jean Marc Boucher. The subject of this article is the denoising of ECGs (realized using wavelets) followed by the segmentation of the result to separate the wave P. A statistical method of segmentation based on hidden Markov chains was used. A first result of the article is the justification of the necessity of denoising. Comparing the results of segmentation obtained with and without denoising it can be observed that the segmentation quality improves if the denoising is associated. The second result is the matching of the denoising technique with the proposed segmentation technique. In this article is proposed a new discrete wavelet transform (with enhanced diversity) that increases the quality of segmentation in comparison with the traditional discrete wavelet transform, DWT. The diploma project of Cristina Stolojescu (PhD student in our department) was realized in a prestigious research laboratory from France. The aim of this project was the classification of noises that affects the electrocardiograms (the base line deformation, the noise due to muscle activity and the noise due the movement of the patient) realized using the ICA in the wavelets domain. The previous achievements of our research team in the field of underground undersea composition identification lie in a number of articles published in the proceedings of some IEEE conferences and in the following paper published in an ISI journal [6] and in some international contracts or grants:

03.2.050.302, 2004-2005, Débruitage des images SONAR en utilisant la théorie des ondelettes: applications aux systèmes d'aide à la décision pour la classification, beneficiary IFREMER Brest, director Moga Sorin, Programme de recherche franco-roumain Brancusi/2005-2006, Débruitage des images SONAR en utilisant la théorie des ondelettes: applications aux systèmes d'aide à la décision pour la classification, beneficiary Foreign Affairs Minister of France and Foreign Affairs Minister of Romania, director Moga Sorin,

2005 2 20742142 2005-2006, Etude sur l'utilisation de la transformée en ondelettes à diversité enrichie pour le débruitage des images SONAR, beneficiary IFREMER Brest.

The articles already mentioned and the research rapports can be consulted at the web address:
http://hermes.etc.upt.ro/cercetare/papers.html .

All these activities refer to SONAR images denoising. We have obtained a large images database from IFREMER Brest. The opinion of the IFREMER specialists concerning our research can be seen at the following web address:
http://www.ifremer.fr/fleet/acous_sism/sonarscope/speckle_filtering.html .
Some new WT were invented and the performances of the best non-linear filters of statistical nature that can be used in the wavelets domain were studied. In the same context can be viewed the following PhD Thesis, belonging to another member of our research team: Firoiu (Adam) Ioana, Reduction du bruit de type speckle par filtrage multi-resolution, advisers -Prof. Jean Marc Boucher and Prof. Isar Alexandru. She works in our department also. Our previous achievements in the field of WiMAX network radio-planning were appeared in the framework of a collaboration of our research team and a similar team from Alcatel-Lucent Timisoara. Because this firm is becoming dealer of WiMAX technology for Romania and South-Eastern Europe, its engineers try to become specialists in this technology. One of their most challenging problems is the design of the WiMAX networks in accordance with the client specifications. On the basis of the topology and quality of services specified by the clients, they must specify the minimum number of equipments and their types. In this respect today are conceived at Alcatel-Lucent Timisoara, software products named tools for the radio-planning of WiMAX networks. These products estimate the operation of the equipment from a specified network based on the propagation conditions, on the performance of the equipment, on the mobiles velocity, on the traffic type and aids at making the decision about the number of users and the decision about the resources allocation for each user. Contrary to the comportment of GSM and UMTS networks, in the case of WiMAX networks the effect of interference is more destructive. This is the reason why our collaboration with the team from Alcatel-Lucent Timisoara started by the quantification of the influence of the interferences on a WiMAX network. We have already written a rapport on this topic [7].

On the basis of those realizations we have fixed the following objectives:
1. – first research year- The study of intelligent techniques for the segmentation and classification of SONAR images based on the association of wavelets with NN. This objective represents a natural continuation of our team researches in the field of denoising SONAR images. A complete system for the aid for decisions making will be obtained by conceiving some segmentation and classification blocks. Its impact in geology field will be very important because it will accelerate significantly the process of decisions making. Despite the fact that the SONAR images segmentation subject is very modern, only a little number of papers was published on this topic. We can mention only the PhD Thesis [8].

This thesis doesn't treat the case of the hyperanalytic wavelet transform. Our intention is to use-it for SONAR images segmentation. We don't know any paper about the SONAR images classification. We want to implement the classification with the aid of NN. The segmentation and classification of SONAR images are very important tasks because a high percent of the Earth surface is covered by water and because due to the development of SONAR technology the number of SONAR images growths exponentially. Obviously this objective has an interdisciplinary character because it supposes the collaboration between geologists and engineers.

The actual research rapport deals with the study of intelligent techniques for the segmentation and classification of SONAR images based on the association of wavelets with NN.

The objective of this grant for the current year is the study of SONAR images intelligent segmentation techniques based on the fusion of wavelets theory and neural networks theory. The correspondent activities are:
- The study of segmentation techniques for textured images obtained after denoising,
- The implementation of the segmentation algorithms obtained at the previous point in Matlab and the simulation of segmentation using SONAR images database whit elements already denoised,
- Conception of a segmentation algorithm for textured images based on the use of the hyperanalytic wavelet transform,
- The implementation of the segmentation algorithm previously obtained in Matlab and the segmentation simulation using a SONAR images database with images already denoised,
- The comparison of results obtained and the classification of the segmentation algorithms based on the type of the denoising used like pre-treatment.

The structure of this rapport follows this sequence of activities. First we introduce in section 2 some statistical segmentation strategies. All these techniques require a statistical model of the wavelet coefficients. For its selection a preliminary statistical analysis of the wavelet coefficients is necessary. We

present such results concerning two wavelet transforms: the discrete wavelet transform and the hyperanalytic wavelet transform.
Next a model having the properties revealed by the statistical analysis can be selected. Some considerations about this selection are presented in section 3. The architectures of some segmentation algorithms are revisited in section 4.

2. Statistical segmentation techniques

When dealing with images segmentation, many authors recommend the use of real or complex wavelet transforms. These decompositions capture the directionality, the structure and the dimensions of the objects embedded in the image under analysis. The objective of the statistical segmentation methods is to select a whole set of parameters from the wavelet coefficients of any pixel of the image analyzed and to compute a distance between this set of parameters and a set of parameters which characterizes a specific region of the image. If this distance is sufficiently small, the current pixel will be associated with the considered region. If not, another specific region will be considered. Basically, there are 2 types of distance which are computed in segmentation applications: the Euclidean distance and the Kulback-Leibler (KL) distance. Generally, the Euclidean distance is used when the set of parameters already mentioned is a features vector. This is a vector composed by some local values of statistical moments computed in a neighborhood centered in the current pixel. For example, the features vector can be formed by the local mean and by the local standard deviation of the current pixel computed in a rectangular neighborhood with size 5×5.

The KL distance is computed between two probability density functions (pdf). Both distances require some statistical models of the "segments" of the image under investigation. Different models of the wavelet coefficients were already tested. The goal of this rapport is to explain how can be constructed a successful model. First, we present a second order statistical analysis of two wavelet transforms (WT) the discrete WT (DWT) and the hyperanalytic WT (HWT). Next we investigate the statistical models which are proposed on the basis of the analysis.

2.1. Second order statistical analysis

We agree the hypothesis that an image can be well statistical modeled like a stationary random process. This assumption makes sufficient a second order statistical analysis. In the following we will analyze first the DWT and second the HWT.

2.1.1. DWT

Let $x(t)$ be a stationary random signal. The DWT coefficients of its projection on a space V_0 are $d_m[n] = \langle x(\tau), \psi_{m,n}(\tau) \rangle$. The correlation of this sequence is:

$$\Gamma_{d_m}[k,l] = E\{d_m[k] d_m^*[l]\} = E\left\{\langle x(\tau), \psi_{m,k}(\tau)\rangle, \langle x(\tau), \psi_{m,l}(\tau)\rangle^*\right\} = \tag{1}$$

$$= E\left\{\int_R x(\tau)\psi_{m,k}^*(\tau)d\tau \int_R x^*(u)\psi_{m,l}(u)du\right\} = \int_{R^2} \mathrm{E}\{x(\tau)x^*(u)\}\psi_{m,k}^*(\tau)\psi_{m,l}(u)d\tau du$$

Because x is stationary:

$$E\{x(\tau)x^*(u)\} = \Gamma_x(\tau - u) \text{ and} \tag{2}$$

$$\Gamma_{d_m}[k,l] = \int_{R^2} \Gamma_x(\tau-u)\psi_{m,k}^*(\tau)\psi_{m,l}(u)d\tau du = \int_R \left(\Gamma_x(\tau) * \psi_{m.l}(\tau)\right)\psi_{m,k}^*(\tau)d\tau.$$

or:

$$\Gamma_{d_m}[k,l] = \int_R \left(\Gamma_x(\tau) * \psi_{m,l}(\tau)\right)\psi^*_{m,k}(\tau)\,d\tau \overset{Parseval}{=} \tag{3}$$

$$= \frac{1}{2\pi}\int_R \mathcal{F}\left\{\Gamma_x(\tau) * \psi_{m,l}(\tau)\right\}(\xi)\mathcal{F}^*\left\{\psi_{m,k}(\tau)\right\}(\xi)\,d\xi.$$

Making the hypothesis that the wavelets are real functions:

$$\Gamma_{d_m}[k,l] = \frac{1}{2\pi}\int_R \mathcal{F}\left\{\Gamma_x(\tau)\right\}(\xi)\mathcal{F}\left\{\psi_{m,l}(\tau)\right\}(\xi)\mathcal{F}^*\left\{\psi_{m,k}(\tau)\right\}(\xi)\,d\xi. \tag{4}$$

But: $\mathcal{F}\left\{\psi_{m,l}(\tau)\right\}(\xi) = 2^{\frac{m}{2}} e^{-j\cdot\xi\cdot 2^m\cdot l}\mathcal{F}\left\{\psi\right\}\left(2^m\xi\right)$ and:

$$\Gamma_{d_m}[k,l] = \frac{1}{2\pi}\int_R \mathcal{F}\left\{\Gamma_x(\tau)\right\}(\xi)2^{\frac{m}{2}} e^{-j\cdot\xi\cdot 2^m\cdot l}\mathcal{F}\left\{\psi\right\}\left(2^m\xi\right)2^{\frac{m}{2}} e^{j\cdot\xi\cdot 2^m\cdot k}\mathcal{F}^*\left\{\psi\right\}\left(2^m\xi\right)d\xi \tag{5}$$

or:

$$\Gamma_{d_m}[k,l] = \frac{1}{2\pi}\int_R \mathcal{F}\left\{\Gamma_x(\tau)\right\}(\xi)2^m e^{-j\cdot\xi\cdot 2^m\cdot(l-k)}\left|\mathcal{F}\left\{\psi\right\}\left(2^m\xi\right)\right|^2 d\xi. \tag{6}$$

The last integral can be decomposed into a series of integrals computed on intervals of length 2π:

$$\Gamma_{d_m}[k,l] = \frac{1}{2\pi}\sum_{p=-\infty}^{\infty}\int_{(2p-1)\pi}^{(2p+1)\pi} \mathcal{F}\left\{\Gamma_x\right\}(\xi)2^m e^{-j\cdot\xi\cdot 2^m\cdot(l-k)}\left|\mathcal{F}\left\{\psi\right\}\left(2^m\xi\right)\right|^2 d\xi. \tag{7}$$

Making the variable change $v = 2^m\xi$, the last equation becomes:

$$\Gamma_{d_m}[k,l] = \frac{1}{2\pi}\sum_{p=-\infty}^{\infty}\int_{(2p-1)\pi}^{(2p+1)\pi} \mathcal{F}\left\{\Gamma_x(\tau)\right\}\left(2^{-m}v\right)e^{-j\cdot(l-k)\cdot v}\left|\mathcal{F}\left\{\psi\right\}(v)\right|^2 dv, \tag{8}$$

or making the second change of variable $w = v - 2p\pi$:

$$\Gamma_{d_m}[k,l] = \frac{1}{2\pi}\int_{-\pi}^{\pi}\sum_{p=-\infty}^{\infty} \mathcal{F}\left\{\Gamma_x(\tau)\right\}\left(2^{-m}\left(w+2p\pi\right)\right)e^{-j\cdot w\cdot(l-k)}\left|\mathcal{F}\left\{\psi\right\}\left(w+2p\pi\right)\right|^2 dw \tag{9}$$

This is a very important result which will be recalled few times in the following.
Tacking the limit for $m \to \infty$, the last relation becomes:

$$\Gamma_{d_\infty}[k,l] = \frac{1}{2\pi}\int_{-\pi}^{\pi} \mathcal{F}\left\{\Gamma_x(\tau)\right\}(0)e^{-j\cdot w\cdot(l-k)}\sum_{p=-\infty}^{\infty}\left|\mathcal{F}\left\{\psi\right\}\left(w+2p\pi\right)\right|^2 dw. \tag{10}$$

Because the sum of the series in the right hand side equals 1 (orthogonal wavelets) it can be written:

$$\Gamma_{d_\infty}[k,l] = \frac{1}{2\pi}\mathcal{F}\left\{\Gamma_x(\tau)\right\}(0)\int_{-\pi}^{\pi} e^{-j\cdot w\cdot(l-k)}dw. \tag{11}$$

The last integral is proportional with the inverse discrete in time Fourier transform of 1(ξ) which equals the sequence $\delta[k-l]$. So, it can be written:

$$\Gamma_{d_\infty}[k,l] = \mathcal{F}\left\{\Gamma_x(\tau)\right\}(0)\delta[k-l]. \tag{12}$$

Hence the sequence $d_\infty[n]$ is not correlated. This is the reason why, asymptotically speaking, it can be said that **the DWT decorrelates its input signal**.
An equation similar to (9) can be written for the approximation coefficients of the DWT:

$$\Gamma_{a_m}[k,l] = \frac{1}{2\pi}\int_{-\pi}^{\pi}\sum_{p=-\infty}^{\infty} \mathcal{F}\left\{\Gamma_x(\tau)\right\}\left(2^{-m}\left(w+2p\pi\right)\right)e^{-j\cdot w\cdot(l-k)}\left|\mathcal{F}\left\{\varphi\right\}\left(w+2p\pi\right)\right|^2 dw \tag{13}$$

The means and the variances of the DWT coefficients are computed in the following. The mean of the detail coefficients is given by:

$$E\{d_m[n]\} = E\{\langle x(t), \psi_{m.k}(t)\rangle\} = E\left\{\int_{-\infty}^{\infty} x(t)\psi^*_{m,k}(t)\,dt\right\} \tag{14}$$

or applying the Fubini's theorem:

$$E\{d_m[k]\} = \int_{-\infty}^{\infty} E\{x(t)\}\psi^*_{m,k}(t)\,dt = \int_{-\infty}^{\infty} \mu_x\psi^*_{m,k}(t)\,dt = \mu_x\mathcal{F}\{\psi^*_{m,k}\}(0). \tag{15}$$

Because, $\mathcal{F}\{\psi_{m,k}\}(\xi) = 2^{-\frac{m}{2}} e^{-j\cdot\xi\cdot 2^{-m}\cdot k}\mathcal{F}\{\psi\}\left(2^{-m}\xi\right)$ the last equation becomes:

$$E\{d_m[k]\} = \mu_x 2^{-\frac{m}{2}}\mathcal{F}\{\psi\}(0). \tag{16}$$

But $\mathcal{F}\{\psi\}(0) = m_1(0)\mathcal{F}\{\varphi\}(0) = m_1(0)$ which equals 0 because m_1 is a high-pass filter. So the mean of each detail coefficients sequence is null.

In what concerns the approximation coefficients, making a similar reasoning:

$$E\{a_m[k]\} = \mu_x\mathcal{F}\{\varphi_{m,k}\}^*(0) \tag{17}$$

or tacking into account the fact that $\mathcal{F}\{\varphi_{m,k}\}(\xi) = 2^{-\frac{m}{2}} e^{-j\cdot\xi\cdot 2^{-m}\cdot k}\mathcal{F}\{\varphi\}\left(2^{-m}\xi\right)$, it can be written:

$$E\{a_m[k]\} = \mu_x 2^{-\frac{m}{2}}\mathcal{F}\{\varphi\}(0) = \mu_x 2^{-\frac{m}{2}}. \tag{18}$$

So, the mean of the approximation coefficients increases with the decomposition level.

The variance of the detail wavelet coefficients can be computed with the aid of their correlation function because they have null statistical mean:

$$E\{d_m^2[k]\} = \Gamma_{d_m}[0] \overset{(9)}{=} \frac{1}{2\pi}\int_R \mathcal{F}\{\Gamma_x\}\left(2^{-m}u\right)\left|\mathcal{F}\{\psi\}(u)\right|^2 du. \tag{19}$$

This is important equation also. Taking the limit for $m \to \infty$ the last equation becomes:

$$E\{d_\infty^2[k]\} = \mathcal{F}\{\Gamma_x\}(0). \tag{20}$$

Hence, asymptotically, the detail wavelet coefficients represent a zero mean white noise with the variance equal with the variance of the input random signal.

The variances of the approximation coefficients are:

$$E\{a_m^2[k]\} = \Gamma_{a_m}[0] - E^2\{a_m[k]\} = \frac{1}{2\pi}\int_R \mathcal{F}\{\Gamma_x\}\left(2^{-m}u\right)\left|\mathcal{F}\{\varphi\}(u)\right|^2 du - 2^m\mu_x^2. \tag{21}$$

So, if x is a stationary random signal with zero mean then the approximation and detail coefficient sequences converge asymptotically (for $m \to \infty$) to zero mean white noises with variance $\mathcal{F}\{\Gamma_x\}(0)$.

Another interesting particular case is that when the signal x is a zero mean white noise with variance σ^2. Then, $\mathcal{F}\{\Gamma_x\}(\xi) = \sigma^2$ and the equation (9) becomes:

$$\Gamma_{d_m}[k,l] = \frac{\sigma^2}{2\pi}\int_{-\pi}^{\pi} e^{-j\cdot w\cdot(l-k)}\sum_{p=-\infty}^{\infty}\left|\mathcal{F}\{\psi\}(w+2p\pi)\right|^2 dw = \sigma^2\delta[k-l] \tag{22}$$

So, all the detail coefficient sequences are zero mean white noises with the same variance equal with the variance of the input signal, $E\{d_m^2[k]\} = \sigma^2$.

Hence the DWT does not correlate the white Gaussian noise.

In the following other equations useful for the construction of denoising systems are derived. The hypothesis of perturbation with AWGN is:

$$x = s + n, \tag{23}$$

where s represents the useful component of the signal to be processed and is considered deterministic and n is a random white Gaussian noise. Then the two terms are not correlated and it can be written:

$$\Gamma_x = \Gamma_s + \Gamma_n \tag{24}$$

Substituting the last equation in (9) it results:

$$\Gamma_{d_m}[k,l] = \frac{1}{2\pi}\int_{-\pi}^{\pi}\sum_{p=-\infty}^{\infty} \mathcal{F}\{\Gamma_s + \Gamma_n\}\left(2^{-m}\left(w+2p\pi\right)\right)e^{-j\cdot w\cdot(l-k)}\left|\mathcal{F}\{\psi\}\left(w+2p\pi\right)\right|^2 dw = \tag{25}$$

$$\frac{1}{2\pi}\int_{-\pi}^{\pi}\sum_{p=-\infty}^{\infty} \mathcal{F}\{\Gamma_s\}\left(2^{-m}\left(w+2p\pi\right)\right)e^{-j\cdot w\cdot(l-k)}\left|\mathcal{F}\{\psi\}\left(w+2p\pi\right)\right|^2 dw + \sigma^2\delta[k-l] =$$

$$= \Gamma_{s d_m}[k,l] + \Gamma_{n d_m}[k,l].$$

and:

$$\Gamma_{s d_m}[k,l] = \frac{1}{2\pi}\int_{-\pi}^{\pi}\sum_{p=-\infty}^{\infty} \mathcal{F}\{\Gamma_s(\tau)\}\left(2^{-m}\left(w+2p\pi\right)\right)e^{-j\cdot w\cdot(l-k)}\left|\mathcal{F}\{\psi\}\left(w+2p\pi\right)\right|^2 dw \tag{26}$$

But:

$$\mathcal{F}\{\Gamma_s\}\left(2^{-m}\left(w+2p\pi\right)\right) = 2^m\mathcal{F}\left\{\Gamma_s\left(2^m\tau\right)\right\}\left(w+2p\pi\right) = \tag{27}$$

$$= 2^m\mathcal{F}\left\{\Gamma_s\left(2^m\tau\right)\cdot e^{-j2p\pi\tau}\right\}(w) = \mathcal{F}\left\{2^m\Gamma_s\left(2^m\tau\right)\right\}(w)$$

and substituting in the last equation:

$$\Gamma_{s d_m}[k,l] = \frac{1}{2\pi}\int_{-\pi}^{\pi}\sum_{p=-\infty}^{\infty} \mathcal{F}\left\{2^m\Gamma_s\left(2^m\tau\right)\right\}(w)\,e^{-j\cdot w\cdot(l-k)}\left|\mathcal{F}\{\psi\}\left(w+2p\pi\right)\right|^2 dw = \tag{28}$$

$$= \frac{1}{2\pi}\int_{-\pi}^{\pi}\mathcal{F}\left\{2^m\Gamma_s\left(2^m\tau\right)\right\}(w)\,e^{-j\cdot w\cdot(l-k)}\cdot\sum_{p=-\infty}^{\infty}\left|\mathcal{F}\{\psi\}\left(w+2p\pi\right)\right|^2 dw =$$

$$= \frac{1}{2\pi}\int_{-\pi}^{\pi}\mathcal{F}\left\{2^m\Gamma_s\left(2^m\tau\right)\right\}(w)\,e^{-j\cdot w\cdot(l-k)}dw = 2^m\Gamma_s\left(2^m\left(l-k\right)\right).$$

The statistical means of the sequences of the detail wavelet coefficients of the useful component of the input signal can be deduced from (16) making the hypothesis: $x=s$ (in the absence of noise, $n=0$ in (23)). It results that these sequences are zero mean:

$$E\{{}_s d_m\} = 0 \tag{29}$$

Finally taking advantage of (29), the variances of those sequences can be computed using their correlations:

$$E\left\{{}_s d_m^2\right\} = \Gamma_{s d_m}[0] = 2^m\Gamma_s(0) \tag{30}$$

It is interesting to observe the relation of the variances of the wavelet detail coefficients of the useful component from two successive scales. Expressing $E\left\{{}_s d_{m-1}^2\right\}$ with relation (30) and comparing the result with $E\left\{{}_s d_m^2\right\}$ it can be written:

$$E\left\{{}_s d_m^2\right\} = \Gamma_{s d_m}[0] = 2E\left\{{}_s d_{m-1}^2\right\} \tag{31}$$

So at any new iteration the variance doubles its value.

2.1.1.1 The 2D-DWT case

At each DWT's iteration the lines of the input image (obtained at the end of the previous iteration) are low-pass filtered with a filter having the impulse response m_0 and high-pass filtered with the filter m_1. Then the lines of the two images obtained at the output of the two filters are decimated with a factor of 2. Next, the columns of the two images obtained are low-pass filtered with m_0 and high-pass filtered with m_1. The columns of those four images are also decimated with a factor of 2. Four new images (representing the result of the current iteration) are obtained. The first sub-image, obtained after two low-pass filtering, is named approximation image (or LL image). The other three are named detail sub-images: LH, HL and HH. The LL sub-image represents the input for the next iteration. In the following, the coefficients of the DWT

will be noted with ${}_xD_m^k$, where x represents the image who's DWT is computed, m represents the iteration index and $k = 1$, for the HH image, $k = 2$, for the HL image, $k = 3$, for the LH image and $k = 4$, for the LL image. These coefficients are computed using the following relation:

$$ {}_xD_m^k[n_1, p_1] = \left\langle x(\tau_1, \tau_2), \psi_{m,n_1,p_1}^k(\tau_1, \tau_2) \right\rangle \tag{32} $$

where the wavelets can be factorized:

$$ \psi_{m,n,p}^k(\tau_1, \tau_2) = \alpha_{m,n}^k(\tau_1) \cdot \beta_{m,p}^k(\tau_2) \tag{33} $$

and the two factors can be computed using the scale function $\varphi(\tau)$ and the mother wavelets $\psi(\tau)$ with the aid of the following relations:

$$ \alpha_{m,n}^k(\tau) = \begin{cases} \varphi_{m,n}(\tau), & k = 1,\ 4 \\ \psi_{m,n}(\tau), & k = 2,\ 3 \end{cases} \tag{34} $$

$$ \beta_{m,p}^k(\tau) = \begin{cases} \varphi_{m,p}(\tau), & k = 2,\ 4 \\ \psi_{m,p}(\tau), & k = 1,\ 3 \end{cases} \tag{35} $$

where:

$$ \begin{aligned} &\varphi_{m,n}(\tau) = 2^{-\frac{m}{2}} \varphi\left(2^{-m}\tau - n\right) \text{ and} \\ &\psi_{m,n}(\tau) = 2^{-\frac{m}{2}} \psi\left(2^{-m}\tau - n\right) \end{aligned} \tag{36} $$

Taking into account (33)-(36) it can be written:

$$ \psi_{m,n,p}^k(\tau_1, \tau_2) = 2^{-m} \psi^k\left(2^{-m}\tau_1 - n, 2^{-m}\tau_2 - p\right) \text{ where } \psi^k(\tau_1, \tau_2) = \psi^k{}_{0,0,0}(\tau_1, \tau_2). \tag{37} $$

The correlation function of the wavelet coefficients can be computed using the following relation:

$$ \Gamma_{{}_xD_m^k}[n_1, n_2, p_1, p_2] = E\left\{ {}_xD_m^k[n_1, p_1] \left({}_xD_m^k[n_2, p_2] \right)^* \right\} \tag{38} $$

Using a computation procedure similar with that used for the derivation of equation (9) it can be obtained:

$$ \begin{aligned} &\Gamma_{{}_xD_m^k}[n_1, n_2, p_1, p_2] = \frac{1}{4\pi^2} \int_{\mathbb{R}^2} \gamma_x\left(2^{-m}\nu_1, 2^{-m}\nu_2\right) \cdot \left| \mathcal{F}\left\{ \psi^k(\nu_1, \nu_2) \right\} \right|^2 \cdot \\ &\cdot e^{-j\left[\nu_1(n_2 - n_1) + \nu_2(p_2 - p_1)\right]} d\nu_1 d\nu_2 \end{aligned} \tag{39} $$

where γ represents the power spectral density of the input signal x and the square of the absolute value representing the second factor in the integral from the right hand side of the last equation is the power spectral density of the mother wavelets which generates the subband k.

Conclusions similar with those obtained analyzing the relation (9) can be expressed after an analysis of the equation (39) when the hypothesis (23) is accepted.

If the input noise is white, with a known variance, σ_n^2 :

$$ \gamma_n\left(2^{-m}\nu_1, 2^{-m}\nu_2\right) = \sigma_n^2 \tag{40} $$

then:

$$ \Gamma_{{}_nD_m^k}[n_1, p_1] = \sigma_n^2 \cdot \delta[n_1] \cdot \delta[p_1]. \tag{41} $$

So, the 2D-DWT does not correlate the white noise, all the detail coefficient sequences are zero mean white noises with the same variance equal with the variance of the input signal σ_n^2.

The same result can be obtained taking in (39) the limit for m tending to infinity. So, asymptotically the 2D DWT transforms every colored noise into a white one. Hence this transform can be regarded as a whitening system.

The first and second order moments of the 2D-DWT wavelet coefficients can be computed using the following relations. The statistical mean can be deduced using arguments similar with those utilized to establish equations (16) and (18):

$$E\left\{{}_{x}D_{m}^{k}\left[n_1,p_1\right]\right\}=E\left\{\int_{\mathbb{R}^2}x\left(\tau_1,\tau_2\right)\cdot\psi_{m,n_1,p_1}^{k*}\left(\tau_1,\tau_2\right)d\tau_1 d\tau_2\right\}=$$
$$\begin{cases}0, & k=1,2,3\\ 2^m\cdot\mu_x, & k=4\end{cases}. \tag{42}$$

Only the means of the images formed with the approximation 2D-DWT wavelet coefficients are not nulls.

The variances can be deduced using arguments similar with those utilized to establish equations (19) and (21):

$$\sigma^2_{{}_{x}D_{m}^{k}}=E\left\{\left|{}_{x}D_{m}^{k}\left[n_1,p_1\right]\right|^2\right\}=\Gamma_{{}_{x}D_{m}^{k}}\left(0,0\right)=$$
$$=\frac{1}{4\pi^2}\int_{\mathbb{R}^2}\gamma_x\left(2^m\nu_1,2^m\nu_2\right)\cdot\left|\mathcal{F}\left\{\psi^k\left(\nu_1,\nu_2\right)\right\}\right|^2 d\nu_1 d\nu_2 \tag{43}$$

The DWT of the input noise component, *n*, has a variance given by:

$$\sigma^2_{{}_{n}D_{m}^{k}}=\begin{cases}\sigma_n^2, & k=1,2,3\\ \sigma_n^2-2^{2m}\mu_n^2, & k=4\end{cases}. \tag{44}$$

Finally, the correlation of the 2D-DWT of *s* is given by:

$$\Gamma_{{}_{s}D_{m}^{k}}\left[n_1,p_1\right]=2^{2m}\cdot\Gamma_s\left[2^m n_1,2^m p_1\right], \tag{45}$$

its mean by:

$$E\left\{{}_{s}D_{m}^{k}\left[n_1,p_1\right]\right\}=\begin{cases}0, & k=1,2,3\\ 2^m\cdot\mu_s, & k=4\end{cases}, \tag{46}$$

and its variance, by:

$$\sigma^2_{{}_{s}D_{m}^{k}}=\begin{cases}2^{2m}\cdot\sigma_s^2 & k=1,2,3\\ 2^{2m}\cdot\sigma_s^2-2^{2m}\mu_s^2, & k=4\end{cases}. \tag{47}$$

So, the variance of the detail wavelet coefficients sequences obtained starting from the useful component of the input image increases when the iteration index increases in each subband (*k*=1,2,3).

2.1.1.2 The probability density function of the wavelet coefficients

In the following the input signal *x* is considered random and is described by the univariate random variable *X* with the pdf $p_X\left(x\right)$. The random variable *Y* obtained by the functional transform $Y=\alpha X$ where α is a constant, has the pdf:

$$p_Y\left(y\right)=\frac{1}{\left|\alpha\right|}p_X\left(\frac{y}{\alpha}\right). \tag{48}$$

So, the random variable *Z* obtained by the functional transform $Z=\sum_{k=1}^{K}\alpha_k X_k$, where α_k are constants and X_k are input random variables, has the pdf:

$$p_Z\left(z\right)=\frac{1}{\left|\alpha_1\right|}f_{X_1}\left(\frac{z}{\alpha_1}\right)*\frac{1}{\left|\alpha_2\right|}f_{X_2}\left(\frac{z}{\alpha_2}\right)*...*\frac{1}{\left|\alpha_K\right|}f_{X_K}\left(\frac{z}{\alpha_K}\right).. \tag{49}$$

For $X_1=X_2=...=X_K=X$ the last equation can be written in the form:

$$p_Z\left(y\right)=\underset{k=1}{\overset{K}{\ast}}\frac{1}{\left|\alpha_k\right|}f_X\left(\frac{y}{\alpha_k}\right). \tag{50}$$

This type of relation can be applied for each of the digital filters composing the DWT computation system. Taking into consideration the fact that the input signal is considered stationary, the decimation blocks belonging to the DWT computation system does not modify the expression of the pdf of the wavelet coefficients and can be omitted. In the following the impulse response of the low pass filters used for the

DWT computation will be denoted by $h=\sqrt{2}m_0$ and the high pass filters by $g=\sqrt{2}m_1$. The random variable which describes the approximation coefficients at the first decomposition level will be denoted by U and the random variable which describes the detail wavelet coefficients will be denoted by Y. Using relations (48)-(50), it can be written:

$$p_U(u)=\underset{k_1=1}{\overset{K}{*}}\frac{1}{|h_{k_1}|}p_X\left(\frac{u}{h_{k_1}}\right)=\frac{1}{\prod_{k_1=1}^{K}|h_{k_1}|}\underset{k_1=1}{\overset{K}{*}}p_X\left(\frac{u}{h_{k_1}}\right)=P_h\underset{k_1=1}{\overset{K}{*}}p_X\left(\frac{u}{h_{k_1}}\right) \tag{51}$$

and:

$$p_Y(y)=P_h^K P_g\underset{k_1=1}{\overset{K}{*}}\underset{k_2=1}{\overset{K}{*}}p_X\left(\frac{y}{h_{k_1}g_{k_2}}\right). \tag{52}$$

The pdf of the detail coefficients obtained after two iterations has the expression:

$$\begin{aligned}p_Y(y)&=P_h^k P_g\underset{k_2=1}{\overset{K}{*}}\underset{k_1=1}{\overset{K}{*}}P_h\underset{k_3=1}{\overset{K}{*}}p_X\left(\frac{y}{h_{k_1}g_{k_2}h_{k_3}}\right)=\\&=P_h^{K+K^2}P_g\underset{k_1=1}{\overset{K}{*}}\underset{k_2=1}{\overset{K}{*}}\underset{k_3=1}{\overset{K}{*}}f_X\left(\frac{y}{h_{k_1}g_{k_2}h_{k_3}}\right).\end{aligned} \tag{53}$$

Finally, the pdf of the detail wavelet coefficients obtained after N iterations can be deduced in a similar way and has the expression:

$$p_Y(y)=P_h^{K+K^2+\ldots+K^N}P_g\underset{k_1=1}{\overset{K}{*}}\underset{k_2=1}{\overset{K}{*}}\ldots\underset{k_{N+1}=1}{\overset{K}{*}}p_X\left(\frac{y}{h_{k_1}h_{k_2}\ldots h_{k_N}g_{k_{N+1}}}\right). \tag{54}$$

The effect of those equations is highlighted by the following simulation where the Haar mother wavelet is considered. In this case:

$$K=2,\ h_1=h_2=g_1=\frac{1}{\sqrt{2}}\ ;g_2=-\frac{1}{\sqrt{2}}\ \Rightarrow\ P_h=2\ ;P_g=2\,. \tag{55}$$

The pdf of the detail wavelet coefficients obtained after the first iteration is given by:

$$p_Y(y)=8\left(p_X(2y)*p_X(2y)*p_X(-2y)*p_X(-2y)\right). \tag{56}$$

In the figure which follows is represented the pdf of the input signal and the pdfs of the approximation and detail coefficients obtained after the first iteration of the DWT. The repartition law of the input signal is of log-Gamma type. The repartition of the input signal is asymmetric. The repartitions of the wavelet coefficients are more symmetric. This effect is more obvious at the second iteration. The repartitions of the coefficients obtained at the second iteration in the same experiment are represented in figure 2.

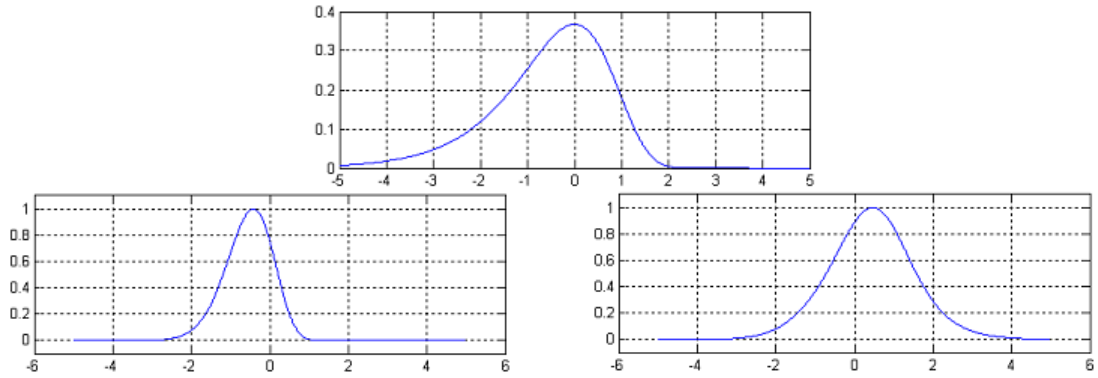

Figure 1. The pdf of the input signal (up) and the pdfs of the approximation (bottom left) and detail (bottom right) coefficients obtained after the first iteration of the DWT computed using the Haar mother wavelets.

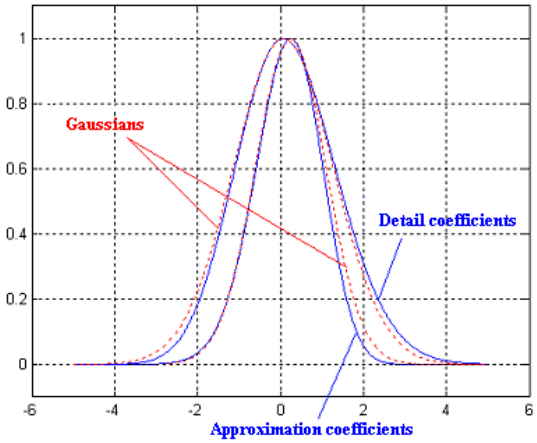

Figure 2. The pdfs of approximation and detail coefficients are close to Gaussians.

This experiment infers the idea that the laws of repartition of the wavelet coefficients are asymptotically Gaussians. In figure 3 is presented the result of another experiment, which confirms this idea.

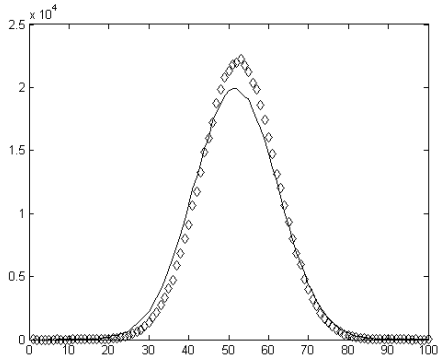

Figure 3. The pdfs of the detail wavelet coefficients (continuous line) after 4 iterations, using a Daubechies mother wavelets with 10 vanishing moments, of a signal distributed following a Gaussian pdf (o line), obtained by simulation with the aid of a histogram.

A theoretical proof of this idea is given in [9].

2.1.2 HWT

The HWT represents a generalization of the analytic wavelet transform, which implementation is presented in figure 2.

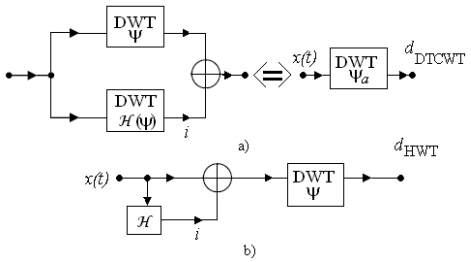

Figure 2. The analytic wavelet transform. a) A dual tree DWT is equivalent with the analytic wavelet transform. b) The analytic wavelet transform can be computed as the DWT of the analytic signal associated to the input signal.

The detail coefficients of the first tree in figure 3 a), which represent the real part of the coefficients of the analytic wavelet transform are:

$$^{1}d_m[n] = \langle x, \psi_{m,n} \rangle ,$$

and the detail coefficients of the second tree in figure 3 a) which represent the imaginary part of the coefficients of the analytic wavelet transform are:

$$^{2}d_m[n] = \langle x, \mathcal{H}\{\psi_{m,n}\} \rangle$$

Their correlation is given by:

$$\begin{aligned}
&\Gamma_{12}[k,l] = E\{ {}^{1}d_m[k], {}^{2}d_m^*[l] \} = \\
&= E\left\{ \langle x(\tau), \psi_{m,k}(\tau) \rangle, \langle x(\tau), \mathcal{H}\{\psi_{m,l}(\tau)\} \rangle^* \right\} = \\
&= E\left\{ \int_R x(\tau) \psi_{m,k}^*(\tau) d\tau \int_R x^*(u) \mathcal{H}\{\psi_{m,l}(u)\} du \right\} = \\
&= \int_{\mathbb{R}^2} E\{x(\tau) x^*(u)\} \psi_{m,k}^*(\tau) \mathcal{H}\{\psi_{m,l}(u)\} d\tau du.
\end{aligned} \tag{57}$$

Because the input signal x is considered stationary the last relation becomes:

$$\begin{aligned}
&\mathcal{E}\{x(\tau) x^*(u)\} = \Gamma_x(\tau - u) \\
&\Gamma_{12}[k,l] = \int_{R^2} \Gamma_x(\tau - u) \psi_{m,k}^*(\tau) \mathcal{H}\{\psi_{m,l}(u)\} d\tau du = \\
&= \int_{\mathbb{R}} \left(\Gamma_x(\tau) * \mathcal{H}\{\psi_{m,l}(\tau)\} \right) \psi_{m,k}^*(\tau) d\tau.
\end{aligned} \tag{58}$$

or:

$$\Gamma_{12}[k,l] = \int_{\mathbb{R}} \left(\Gamma_x(\tau) * \mathcal{H}\{\psi_{m,l}(\tau)\} \right) \psi_{m,k}^*(\tau) d\tau \overset{Parseval}{=} \frac{1}{2\pi} \int_{\mathbb{R}} \mathcal{F}\{\Gamma_x(\tau) * \mathcal{H}\{\psi_{m,l}(\tau)\}\}(\xi) \mathcal{F}^*\{\psi_{m,k}(\tau)\}(\xi) d\xi.$$

If the wavelets are real functions, the last relation becomes:

$$\begin{aligned}
&\Gamma_{12}[k,l] = \frac{1}{2\pi} \int_{\mathbb{R}} \mathcal{F}\{\Gamma_x(\tau)\}(\xi) \mathcal{F}\{\mathcal{H}\{\psi_{m,l}(\tau)\}\}(\xi) \mathcal{F}^*\{\psi_{m,k}(\tau)\}(\xi) d\xi = \\
&= \frac{1}{2\pi} \int_{\mathbb{R}} (-j\, sgn\, \xi) \mathcal{F}\{\Gamma_x(\tau)\}(\xi) \mathcal{F}\{\psi_{m,l}(\tau)\}(\xi) \mathcal{F}^*\{\psi_{m,k}(\tau)\}(\xi) d\xi
\end{aligned} \tag{59}$$

But:

$$\mathcal{F}\{\psi_{m,l}(\tau)\}(\xi) = 2^{\frac{m}{2}} e^{-j \cdot \xi \cdot 2^m \cdot l} \mathcal{F}\{\psi\}(2^m \xi) \tag{60}$$

and:

$$\Gamma_{12}[k,l] = \frac{1}{2\pi} \int_{\mathbb{R}} (-j\, sgn\, \xi) \mathcal{F}\{\Gamma_x(\tau)\}(\xi) 2^{\frac{m}{2}} e^{-j \cdot \xi \cdot 2^m \cdot l} \mathcal{F}\{\psi\}(2^m \xi) 2^{\frac{m}{2}} e^{j \cdot \xi \cdot 2^m \cdot k} \mathcal{F}^*\{\psi\}(2^m \xi) d\xi$$

or:

$$\begin{aligned}
&\Gamma_{12}[k,l] = \frac{1}{2\pi} \int_{\mathbb{R}} (-j\, sgn\, \xi) \mathcal{F}\{\Gamma_x(\tau)\}(\xi) 2^m e^{-j \cdot \xi \cdot 2^m \cdot (l-k)} \left| \mathcal{F}\{\psi\}(2^m \xi) \right|^2 d\xi = \\
&= \frac{1}{2\pi} \int_{R} \mathcal{F}\{\mathcal{H}\{\Gamma_x(\tau)\}\}(\xi) 2^m e^{-j \cdot \xi \cdot 2^m \cdot (l-k)} \left| \mathcal{F}\{\psi\}(2^m \xi) \right|^2 d\xi.
\end{aligned} \tag{61}$$

The last integral can be decomposed into a series of integrals computed on intervals of length 2π:

$$\Gamma_{12}[k,l] = \frac{1}{2\pi} \sum_{p=-\infty}^{\infty} \int_{(2p-1)\pi}^{(2p+1)\pi} \mathcal{F}\{\mathcal{H}\{\Gamma_x\}\}(\xi) 2^m e^{-j \cdot \xi \cdot 2^m \cdot (l-k)} \left| \mathcal{F}\{\psi\}(2^m \xi) \right|^2 d\xi. \tag{62}$$

After the change of variable $v = 2^m \xi$ the last equation becomes:

$$\Gamma_{12}[k,l]=\frac{1}{2\pi}\sum_{p=-\infty}^{\infty}\int_{(2p-1)\pi}^{(2p+1)\pi}\mathcal{F}\left\{\mathcal{H}\left\{\Gamma_x(\tau)\right\}\right\}\left(2^{-m}v\right)e^{-j\cdot(l-k)\cdot v}\left|\mathcal{F}\{\psi\}(v)\right|^2 dv \tag{63}$$

or making another change of variable, $w=v-2p\pi$,

$$\Gamma_{12}[k,l]=\frac{1}{2\pi}\int_{-\pi}^{\pi}\sum_{p=-\infty}^{\infty}\mathcal{F}\left\{\mathcal{H}\left\{\Gamma_x(\tau)\right\}\right\}\left(2^{-m}\left(w+2p\pi\right)\right)e^{-j\cdot w\cdot(l-k)}\left|\mathcal{F}\{\psi\}(w+2p\pi)\right|^2 dw\,. \tag{64}$$

Tacking the limit for $m\to\infty$, it results:

$$\Gamma_{12_\infty}[k,l]=\frac{1}{2\pi}\int_{-\pi}^{\pi}\mathcal{F}\left\{\mathcal{H}\left\{\Gamma_x(\tau)\right\}\right\}(0)e^{-j\cdot w\cdot(l-k)}\sum_{p=-\infty}^{\infty}\left|\mathcal{F}\{\psi\}(w+2p\pi)\right|^2 dw.\,. \tag{65}$$

Because the Fourier transform of the Hilbert transform of any signal equals 0 at $\xi=0$, it can be written:

$$\Gamma_{12_\infty}[k,l]=0\,. \tag{66}$$

So, asymptotically, the real and imaginary parts of the analytic wavelet transform coefficients are decorrelated like consequence of the utilization of the Hilbert transform.

The HWT implementation is presented in figure 3. For each 2DDWT, the conclusions of the statistical analysis of the DWT already presented in section 2.3.2.1.1 are applicable. Comparing figures 2 and 3 it can be observed that the system composed by the first two trees in figure 3 has architecture similar with that of the analytic wavelet transform. So, the coefficients obtained at the outputs of the first two trees implementing the HWT are asymptotically decorrelated. The system composed by the last two trees in figure 3 has also architecture similar with that presented in figure 2 a). Hence, the coefficients obtained at the outputs of the last two trees implementing the HWT are also asymptotically decorrelated. A similar reasoning proves that the outputs of the first and third tree or the outputs of the second and the forth tree are also asymptotically decorrelated.

In the following are analyzed the complex coefficients z_+ and z_-, obtained after the directional selectivity enhancement, which real and imaginary parts are:

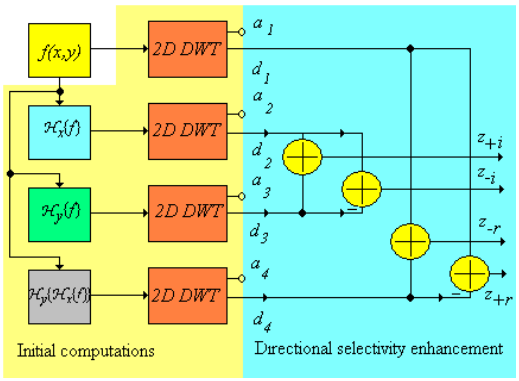

Figure 3. The architecture of the HWT computation system.

$$z_{+i}=d_2+d_3\;;\;z_{-i}=d_2-d_3\;;\;z_{-r}=d_1+d_4\;\text{ and }\;z_{+r}=d_1-d_4\,. \tag{67}$$

These coefficients are computed using the following type of relation:

$${}^{+i}_{f}z^k_m[n_1,p_1]={}^{2}_{f}D^k_m[n_1,p_1]+{}^{3}_{f}D^k_m[n_1,p_1]=\left\langle\mathcal{H}_x\{f\}(\tau_1,\tau_2)+\mathcal{H}_y\{f\}(\tau_1,\tau_2),\psi^k_{m,n_1,p_1}(\tau_1,\tau_2)\right\rangle$$

The correlation function of the wavelet coefficients can be computed using the following relation:

$$\Gamma_{{}^{+i}_{f}z^{k}_{m}}[n_1,n_2,p_1,p_2]=E\left\{{}^{+i}_{f}z^{k}_{m}[n_1,p_1]\left({}^{+i}_{f}z^{k}_{m}[n_2,p_2]\right)^{*}\right\}=$$

$$=E\left\{\left\langle\mathcal{H}_x\{f\}(\tau_1,\tau_2)+\mathcal{H}_y\{f\}(\tau_1,\tau_2),\psi^{k}_{m,n_1,p_1}(\tau_1,\tau_2)\right\rangle\cdot\right.$$

$$\left.\left(\left\langle\mathcal{H}_x\{f\}(\tau_1,\tau_2)+\mathcal{H}_y\{f\}(\tau_1,\tau_2),\psi^{k}_{m,n_2,p_2}(\tau_1,\tau_2)\right\rangle\right)^{*}\right\}=$$

$$=E\left\{\left(\left\langle\mathcal{H}_x\{f\}(\tau_1,\tau_2),\psi^{k}_{m,n_1,p_1}(\tau_1,\tau_2)\right\rangle+\left\langle\mathcal{H}_y\{f\}(\tau_1,\tau_2),\psi^{k}_{m,n_1,p_1}(\tau_1,\tau_2)\right\rangle\right)\cdot\right.$$

$$\left.\cdot\left(\left\langle\mathcal{H}_x\{f\}(\tau_1,\tau_2),\psi^{k}_{m,n_2,p_2}(\tau_1,\tau_2)\right\rangle+\left\langle\mathcal{H}_y\{f\}(\tau_1,\tau_2),\psi^{k}_{m,n_2,p_2}(\tau_1,\tau_2)\right\rangle\right)^{*}\right\}=$$

$$=E\left\{\left\langle\mathcal{H}_x\{f\}(\tau_1,\tau_2),\psi^{k}_{m,n_1,p_1}(\tau_1,\tau_2)\right\rangle\cdot\left\langle\mathcal{H}_x\{f\}(\tau_1,\tau_2),\psi^{k}_{m,n_2,p_2}(\tau_1,\tau_2)\right\rangle^{*}\right\}+ \tag{68}$$

$$+E\left\{\left\langle\mathcal{H}_x\{f\}(\tau_1,\tau_2),\psi^{k}_{m,n_1,p_1}(\tau_1,\tau_2)\right\rangle\cdot\left\langle\mathcal{H}_y\{f\}(\tau_1,\tau_2),\psi^{k}_{m,n_2,p_2}(\tau_1,\tau_2)\right\rangle^{*}\right\}+$$

$$+E\left\{\left\langle\mathcal{H}_y\{f\}(\tau_1,\tau_2),\psi^{k}_{m,n_1,p_1}(\tau_1,\tau_2)\right\rangle\cdot\left\langle\mathcal{H}_x\{f\}(\tau_1,\tau_2),\psi^{k}_{m,n_2,p_2}(\tau_1,\tau_2)\right\rangle^{*}\right\}+$$

$$E\left\{\left\langle\mathcal{H}_y\{f\}(\tau_1,\tau_2),\psi^{k}_{m,n_1,p_1}(\tau_1,\tau_2)\right\rangle\cdot\left\langle\mathcal{H}_y\{f\}(\tau_1,\tau_2),\psi^{k}_{m,n_2,p_2}(\tau_1,\tau_2)\right\rangle^{*}\right\}$$

Each term of the right hand side can be written in the form given in (39) because it is a result of a 2D DWT:

$$E\left\{\left\langle\mathcal{H}_x\{f\}(\tau_1,\tau_2),\psi^{k}_{m,n_1,p_1}(\tau_1,\tau_2)\right\rangle\cdot\left\langle\mathcal{H}_x\{f\}(\tau_1,\tau_2),\psi^{k}_{m,n_2,p_2}(\tau_1,\tau_2)\right\rangle^{*}\right\}= \tag{69}$$

$$\frac{1}{4\pi^2}\int_{\mathbb{R}^2}\gamma_{\mathcal{H}_x\{f\}}\left(2^{-m}\nu_1,2^{-m}\nu_2\right)\cdot\left|\mathcal{F}\left\{\psi^{k}(\nu_1,\nu_2)\right\}\right|^2\cdot e^{-j\left[\nu_1(n_2-n_1)+\nu_2(p_2-p_1)\right]}d\nu_1d\nu_2$$

$$E\left\{\left\langle\mathcal{H}_x\{f\}(\tau_1,\tau_2),\psi^{k}_{m,n_1,p_1}(\tau_1,\tau_2)\right\rangle\cdot\left\langle\mathcal{H}_y\{f\}(\tau_1,\tau_2),\psi^{k}_{m,n_2,p_2}(\tau_1,\tau_2)\right\rangle^{*}\right\}+= \tag{70}$$

$$\frac{1}{4\pi^2}\int_{\mathbb{R}^2}\gamma_{\mathcal{H}_x\{f\}\mathcal{H}_y\{f\}}\left(2^{-m}\nu_1,2^{-m}\nu_2\right)\cdot\left|\mathcal{F}\left\{\psi^{k}(\nu_1,\nu_2)\right\}\right|^2\cdot e^{-j\left[\nu_1(n_2-n_1)+\nu_2(p_2-p_1)\right]}d\nu_1d\nu_2$$

$$E\left\{\left\langle\mathcal{H}_y\{f\}(\tau_1,\tau_2),\psi^{k}_{m,n_1,p_1}(\tau_1,\tau_2)\right\rangle\cdot\left\langle\mathcal{H}_x\{f\}(\tau_1,\tau_2),\psi^{k}_{m,n_2,p_2}(\tau_1,\tau_2)\right\rangle^{*}\right\}= \tag{71}$$

$$\frac{1}{4\pi^2}\int_{\mathbb{R}^2}\gamma_{\mathcal{H}_y\{f\}\mathcal{H}_x\{f\}}\left(2^{-m}\nu_1,2^{-m}\nu_2\right)\cdot\left|\mathcal{F}\left\{\psi^{k}(\nu_1,\nu_2)\right\}\right|^2\cdot e^{-j\left[\nu_1(n_2-n_1)+\nu_2(p_2-p_1)\right]}d\nu_1d\nu_2$$

and:

$$E\left\{\left\langle\mathcal{H}_y\{f\}(\tau_1,\tau_2),\psi^{k}_{m,n_1,p_1}(\tau_1,\tau_2)\right\rangle\cdot\left\langle\mathcal{H}_y\{f\}(\tau_1,\tau_2),\psi^{k}_{m,n_2,p_2}(\tau_1,\tau_2)\right\rangle^{*}\right\}= \tag{72}$$

$$\frac{1}{4\pi^2}\int_{\mathbb{R}^2}\gamma_{\mathcal{H}_y\{f\}\mathcal{H}_x\{f\}}\left(2^{-m}\nu_1,2^{-m}\nu_2\right)\cdot\left|\mathcal{F}\left\{\psi^{k}(\nu_1,\nu_2)\right\}\right|^2\cdot e^{-j\left[\nu_1(n_2-n_1)+\nu_2(p_2-p_1)\right]}d\nu_1d\nu_2$$

In consequence:

$$\Gamma_{{}^{+i}_{f}z^{k}_{m}}[n_1,n_2,p_1,p_2]=\frac{1}{4\pi^2}\int_{\mathbb{R}^2}\left(\gamma_{\mathcal{H}_x\{f\}}+\gamma_{\mathcal{H}_x\{f\}\mathcal{H}_y\{f\}}+\gamma_{\mathcal{H}_y\{f\}\mathcal{H}_x\{f\}}+\gamma_{\mathcal{H}_y\{f\}}\right)\left(2^{-m}\nu_1,2^{-m}\nu_2\right)\cdot$$

$$\cdot\left|\mathcal{F}\left\{\psi^{k}(\nu_1,\nu_2)\right\}\right|^2\cdot e^{-j\left[\nu_1(n_2-n_1)+\nu_2(p_2-p_1)\right]}d\nu_1d\nu_2$$

But:

$$\gamma_{\mathcal{H}_x\{f\}}(\xi_1,\xi_2)=\left|\mathcal{F}\left\{\mathcal{H}_x\{f\}\right\}\right|^2(\xi_1,\xi_2)=\left|sgn\,\xi_1\right|^2\left|\mathcal{F}\{f\}(\xi_1,\xi_2)\right|^2=\left|sgn\,\xi_1\right|^2\cdot\gamma_f(\xi_1,\xi_2),$$

$$\gamma_{\mathcal{H}_x\{f\}\mathcal{H}_y\{f\}}(\xi_1,\xi_2)=\mathcal{F}\left\{\mathcal{H}_x\{f\}\right\}(\xi_1,\xi_2)\cdot\mathcal{F}^*\left\{\mathcal{H}_y\{f\}\right\}(\xi_1,\xi_2)=$$

$$=\left(-j\,sgn\,\xi_1\right)\mathcal{F}\{f\}(\xi_1,\xi_2)\left[\left(-j\,sgn\,\xi_2\right)\mathcal{F}\{f\}(\xi_1,\xi_2)\right]^*=$$

$$=sgn\,\xi_1\cdot sgn\,\xi_2\cdot\left|\mathcal{F}\{f\}(\xi_1,\xi_2)\right|^2=sgn\,\xi_1\cdot sgn\,\xi_2\cdot\gamma_f(\xi_1,\xi_2),$$

$$\gamma_{\mathcal{H}_y\{f\}\mathcal{H}_x\{f\}}(\xi_1,\xi_2)=\mathcal{F}\left\{\mathcal{H}_y\{f\}\right\}(\xi_1,\xi_2)\cdot\mathcal{F}^*\left\{\mathcal{H}_x\{f\}\right\}(\xi_1,\xi_2)=$$

$$\left(-j\,sgn\,\xi_2\right)\mathcal{F}\{f\}(\xi_1,\xi_2)\left[\left(-j\,sgn\,\xi_1\right)\mathcal{F}\{f\}(\xi_1,\xi_2)\right]^*=$$

$$=sgn\,\xi_1\cdot sgn\,\xi_2\cdot\left|\mathcal{F}\{f\}(\xi_1,\xi_2)\right|^2=sgn\,\xi_1\cdot sgn\,\xi_2\cdot\gamma_f(\xi_1,\xi_2),$$

$$\gamma_{\mathcal{H}_y\{f\}}=\left|\left(-j\,sgn\,\xi_2\right)\mathcal{F}\{f\}(\xi_1,\xi_2)\right|^2=\left|sgn\,\xi_2\right|^2\cdot\gamma_f(\xi_1,\xi_2).$$

So:

$$\begin{aligned}&\Gamma_{{}^{+i}_{f}z^{k}_{m}}[n_1,n_2,p_1,p_2]=\frac{1}{4\pi^2}\cdot\\&\cdot\int_{\mathbb{R}^2}\left[\left(\left|sgn\,\xi_1\right|^2+2\,sgn\,\xi_1\,sgn\,\xi_2+\left|sgn\,\xi_2\right|^2\right)\gamma_f(\xi_1,\xi_2)\right]\left(\xi_1=2^{-m}\nu_1,\xi_2=2^{-m}\nu_2\right)\cdot\\&\cdot\left|\mathcal{F}\left\{\psi^k(\nu_1,\nu_2)\right\}\right|^2\cdot e^{-j\left[\nu_1(n_2-n_1)+\nu_2(p_2-p_1)\right]}d\nu_1 d\nu_2\end{aligned}\tag{73}$$

The asymptotic comportment of the coefficients z_{+i} can be obtained if the limit for $m\to\infty$ is taken into the last relation:

$$\Gamma_{{}^{+i}_{f}z^{k}_{\infty}}[n_1,n_2,p_1,p_2]=0,\tag{74}$$

because $sgn\,0=0$.

Similar considerations can be made for the other coefficients, z_{+r} , z_{-i} and z_{-r}. Hence, asymptotically the detail coefficients of the HWT are decorrelated.

Further consideration can be made following the same line of reasoning about the first two moments of the coefficients z and about the case when the input image is AWGN.

So, the HWT has a statistical comportment similar with that of the 2D DWT but has better translation invariance and directional selectivity [10]. If an increased directional selectivity is required (this can be the case when the image to be segmented contains a lot of textural regions) then a better solution could be the Hyperanalytic Wavelet Packets Transform (HWPT) [11].

3. The selection of the statistical model of the wavelet coefficients

There are a lot of models which can be selected for the wavelet coefficients. The model of wavelet coefficients of natural images is given by heavy tailed distributions, [12]. These models can be classified as marginal (when a univariate random variable is used to model the wavelet coefficients) or global (when a bivariate random variable is used). The marginal distributions are typically long tailed with high kurtosis (fourth moment divided by the variance squared). The shape, including the sharp peak at zero and the long tails, is the statistical manifestation of the sparseness property of wavelet coefficients. The marginal models start from the histograms of the wavelet coefficients and try to find the model which best feats these histograms. To highlight the heavy tailed distributions which characterize the HWT coefficients, the following experiment was done. The histograms of the different subbands obtained applying the HWT to the image Lena are computed. The results are represented in the following figure. The linear dependencies of the two branches of the logarithms of the histograms prove that the pdfs of the real and imaginary parts of the HWT coefficients correspond to exponential laws (which are heavy tailed):

$$\log\left(K_1\cdot e^{-|x|}\right)=K_2-|x|\tag{75}$$

where K_1 and K_2 represent two constants. So, the hypothesis that the real and imaginary parts of the useful HWT coefficients are distributed following Laplace laws can be made.

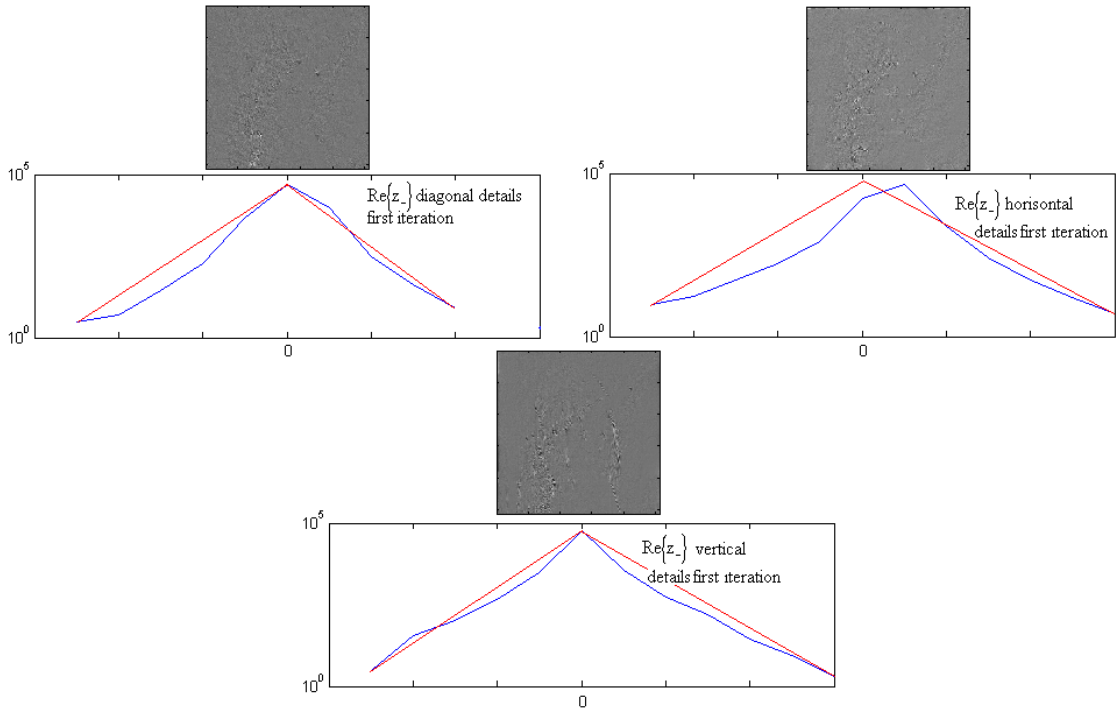

Figure 2. The histograms of some subbands of the HWT of the image Lena computed using the mother wavelets Dau_20 are represented semi logarithmically (on the vertical axe are represented the logarithms of the values of the histograms) in blue. The corresponding linear dependencies are represented in red.

Some examples of marginal distributions of the wavelet coefficients are: the Generalized Gaussian (GG) model, proposed by Mallat [13], the Laplacian distribution proposed by Selesnick [12], Asymmetric Generalized Gaussian density (AGG) [14] etc. These repartition laws have same parameters which are estimated locally, for each pixel of the image which must be segmented, using its WT coefficients. The vector of those parameters represents the vector features associated to the current pixel. The marginal models do not take into account the intra-scale and the inter-scale dependencies of the wavelet coefficients. For this reason were conceived bi-variate models for the wavelet coefficients. The best were constructed with the aid of the Gaussian Scale Mixture (GSM) model. In the following is presented the construction of a bivariate model starting from the GSM.

3.1. Interscale dependence

In the case of DWT a strong interscale dependence was observed. The wavelet coefficients of natural images display a self-reinforcing characteristic in that if one coefficient is large in magnitude, then other coefficients in its neighborhood are also likely to be large in magnitude (intrascale dependence). The intuitive explanation for this is that localized image structures such as edges have substantial power across many scales and nearby spatial locations at a given orientation. The wavelet coefficients that represent the image will also have large magnitudes at these scales; locations and orientation (interscale dependence). However, the signs and relative magnitudes of these coefficients will depend on the exact shape, location and orientation of the structure. Each wavelet coefficient w_1 has a parent w_2, situated in the same geometric position but at the next coarser scale. The interscale dependence means that if a parent coefficient is large then its child coefficient is also large. The inclusion of coefficients at the parent scale in the model of the wavelet coefficients is used to capture the 'persistence across scale' characteristic. The construction of the bivariate pdf can be done with the aid of Gaussian Scale Mixtures (GSM). This simple statistical model has been used to model natural signals such as speech and more recently to describe the non-stationary behavior of the wavelet coefficients of natural images and is given in equation (76). It assumes that each

vector of coefficients **w** is specified by a stationary bivariate zero mean Gaussian process **x** and a spatially fluctuating variance *z*:

$$\mathbf{w} = \sqrt{z} \cdot \mathbf{x}, \quad z \in \mathrm{R}, \quad \mathbf{w}, \mathbf{x} \in \mathrm{R}^d . \tag{76}$$

The multiplier *z* is usually a function of the surrounding coefficient values (like the local variance of the coefficients within the same scale or a more complex function of the neighboring coefficients within the same and adjacent scales). The result is always leptokurotic (kurtosis ≥ 3), its distribution having long tails.

To model the self-reinforcing property of the coefficients, *z* must be slowly varying but need not be symmetric in all directions. It has been shown that for slowly varying *z* this model can successfully simulate the high kurtosis and longer tails of the marginal distributions. The stationary portion of the model **x** is Gaussian distributed over a small neighborhood of wavelet coefficients. It is generally assumed that *z* varies slowly enough to be considered constant over that neighborhood of coefficients. Under this assumption the model is now a particular form of a spherically invariant random process called a GSM.
For a small neighborhood of coefficients at nearby spatial locations and scale, a GSM vector **w** is the product of two independent random variables: a positive scalar *z* referred to as the hidden multiplier or mixing variable and a Gaussian random vector **x**. The pdf of the Gaussian vector **x** is given by:

$$p_{\mathbf{x}}(\mathbf{x}) = \frac{1}{\left(2\pi\sigma^2\right)^{d/2}} \cdot e^{-\frac{\|x\|^2}{2\sigma^2}}, \tag{77}$$

Setting $a = \sqrt{z}$, then $\mathbf{w} = a \cdot \mathbf{x}$ and the pdf of the random vector **w** is given by:

$$p_{\mathbf{w}}(\mathbf{w}) = \int_0^\infty p_a(a) \cdot \frac{1}{a^d} \cdot p_{\mathbf{x}}\left(\frac{\mathbf{w}}{a}\right) da , \tag{78}$$

Tacking into account the relation of *a* and *z*, the pdf of *a* can be expressed on the basis of the pdf of *z*:

$$p_a(a) = \frac{p_z(z)}{\frac{da}{dz}} = \frac{p_z\left(a^2\right)}{\frac{1}{2a}} = 2a \cdot p_z\left(a^2\right). \tag{79}$$

Substituting (77) into (78), the expression of the pdf of **w** becomes:

$$P_{\mathbf{w}}(\mathbf{w}) = = \int_0^\infty 2a p_z\left(a^2\right) \cdot \frac{1}{a^d} \cdot p_{\mathbf{x}}(\mathbf{w}/a) da. \tag{80}$$

It remains to specify the prior probability function $p_z(z)$ for the multiplier *z*.

3.1.1 Bivariate pdfs

Some propositions of prior probability functions are made in [15]. One of these propositions is the Gamma law:

$$p_z(z) = \frac{\beta^\alpha}{\Gamma(\alpha)} \cdot z^{\alpha-1} \cdot e^{-\beta z} \text{ with } \alpha = \beta = \frac{d+1}{2} . \tag{81}$$

Substituting (81) in (80), the expression of the pdf of **w** becomes:

$${}^1p_{\mathbf{w}}(\mathbf{w}) = \frac{2(\beta)^\alpha}{\Gamma(\alpha)} \int_0^\infty a \cdot a^{2(\alpha-1)} \cdot e^{-\beta a^2} \cdot \frac{1}{a^d} \cdot \frac{1}{\left(2\pi\sigma^2\right)^{\frac{d}{2}}} \cdot e^{-\frac{\|\mathbf{w}\|^2}{2a^2\sigma^2}} da , \tag{82}$$

or taking into account the values of the parameters α and β:

$${}^1p_{\mathbf{w}}(\mathbf{w}) = \frac{2\left(\frac{d+1}{2}\right)^{\frac{d+1}{2}}}{\Gamma\left(\frac{d+1}{2}\right)} \int_0^\infty a \cdot a^{2(d-1)/2} \cdot e^{-\left(\frac{d+1}{2}\right)a^2} \cdot \frac{1}{a^d} \cdot \frac{1}{\left(2\pi\sigma^2\right)^{\frac{d}{2}}} \cdot e^{-\frac{\|\mathbf{w}\|^2}{2a^2\sigma^2}} da. \tag{83}$$

Finally:

$$ {}^1p_{\mathbf{w}}(\mathbf{w}) = \frac{2}{\Gamma\left(\frac{d+1}{2}\right)} \cdot \left(\frac{d+1}{2}\right)^{\frac{d+1}{2}} \cdot \frac{1}{\left(2\pi\sigma^2\right)^{\frac{d}{2}}} \cdot \int_0^{\infty} e^{-\frac{d+1}{2}a^2 - \frac{\|\mathbf{w}\|^2}{2\sigma^2 a^2}} da \tag{84} $$

The last integral can be computed using the following identity:

$$ \int_0^{\infty} e^{-K_1 a^2 - \frac{K_2}{a^2}} da = \frac{1}{2}\sqrt{\frac{\pi}{K_1}} e^{-2\sqrt{K_1 K_2}} \tag{85} $$

Giving to the constants K_1 and K_2 the values: $K_1 = \frac{d+1}{2}$ and $K_2 = \frac{\|\mathbf{w}\|^2}{2\sigma^2}$ the expression of the pdf of **w** can be put in the form:

$$ {}^1p_{\mathbf{w}}(\mathbf{w}) = \frac{2}{\Gamma\left(\frac{d+1}{2}\right)} \cdot \left(\frac{d+1}{2}\right)^{\frac{d+1}{2}} \cdot \frac{1}{\left(2\pi\sigma^2\right)^{\frac{d}{2}}} \cdot \sqrt{\frac{\pi}{\frac{d+1}{2}}} \cdot e^{-\frac{\sqrt{d+1}}{\sigma}\|\mathbf{w}\|} \tag{86} $$

This is a *d*-dimensional spherically-contoured multivariate pdf [15].
For *d*=2, this pdf is bivariate:

$$ {}^1p_{\mathbf{w}}(\mathbf{w}) = \frac{3}{2\pi\sigma^2} \cdot e^{-\frac{\sqrt{3}}{\sigma}\cdot\sqrt{w_1^2+w_2^2}}. \tag{87} $$

For *d*=1, the pdf in (86) is univariate:

$$ {}^1p_w(w) = \frac{\sqrt{2}}{\sigma} \cdot e^{-\frac{\sqrt{2}}{\sigma}\cdot|w|} \tag{88} $$

This univariate pdf is of the form of the Laplace law. In consequence the GSM hypothesis, even for the case of a unique scale, is useful for modeling the repartition of the wavelet coefficients.
The joint pdf from (87) is proportional with the product of two univariate pdfs of Laplace type:

$$ {}^1p_{\mathbf{w}}(w_1,w_2) = \frac{3}{2\pi\sigma^2} \cdot e^{-\frac{\sqrt{3}}{\sigma}\cdot\sqrt{w_1^2+w_2^2}} = \sqrt{\frac{3}{2\pi}}\frac{1}{\sigma}e^{-\frac{\sqrt{3}}{\sigma}\cdot|w_1|} \sqrt{\frac{3}{2\pi}}\frac{1}{\sigma}e^{-\frac{\sqrt{3}}{\sigma}\cdot|w_2|} = K\,{}^1p_{w_1}(w_1)\cdot K\,{}^1p_{w_2}(w_2) \tag{89} $$

which can be regarded as marginal distributions of the corresponding wavelet coefficients at the considered successive scales. *K* represents a constant. Because:

$$ {}^1p_{\mathbf{w}}(w_1,w_2) \neq {}^1p_{w_1}(w_1)\cdot{}^1p_{w_2}(w_2), \tag{90} $$

the random variables w_1 and w_2 are not independent. So, the hypothesis of the univariate Laplace law for the marginal distribution of the wavelet coefficients already analyzed is in accord with the model in (87).

Other proposition of prior probability function made in [15] is the exponential $p_z(z) = e^{-z}$ for $z \geq 0$. In the following table are presented the wavelet coefficients bivariate distribution models corresponding to the different pdfs for the vector **x** constructed with the exponential prior.

Table 1.3.1.1. Two bivariate distribution models for the wavelet coefficients constructed in [15] and their corresponding $p_{\mathbf{x}}(\mathbf{x})$ pdfs.

No.	$p_{\mathbf{x}}(\mathbf{x})$	$p_{\mathbf{w}}(\mathbf{w})$	Remarks
1	$\frac{1}{2\pi\sigma^2}\cdot e^{-\frac{x_1^2+x_2^2}{2\sigma^2}}$	${}^2p_{\mathbf{w}}(\mathbf{w}) = \frac{1}{\pi\sigma^2}K_0\left(\frac{\sqrt{2}}{\sigma}\sqrt{w_1^2+w_2^2}\right)$	$K_\lambda(u) = \frac{1}{2}\cdot\left(\frac{u}{2}\right)^{\lambda}\cdot\int_0^{\infty} t^{-\lambda-1}\cdot e^{-t-\frac{u^2}{4t}}dt$
2	$\frac{1}{2\pi\sigma_1\sigma_2}\cdot e^{-\frac{1}{2}\left(\frac{x_1^2}{\sigma_1^2}+\frac{x_2^2}{\sigma_2^2}\right)}$	${}^3p_{\mathbf{w}}(\mathbf{w})\frac{1}{\pi\sigma_1\sigma_2}K_0\left(\sqrt{2\left(\frac{w_1^2}{\sigma_1^2}+\frac{w_2^2}{\sigma_2^2}\right)}\right)$	$K_0(u) = \frac{1}{2}\cdot\int_0^{\infty} t^{-1}\cdot e^{-t-\frac{u^2}{4t}}dt$

The model in the first line of the table is also a spherically-contoured bivariate pdf. The model in the second line represents an elliptically-contoured bivariate pdf. The GSM model was also used for the conception of one of the best denoising methods [16]. The prior probability function proposed in this

reference is $p_z(z)=\frac{1}{z}$, for $z\geq 0$. It must be remarked that strictly speaking this is not a pdf. Substituting this function in (79) and supposing that the pdf of the Gaussian vector is that given in (77) it can be written:

$$ {}^4p_{\mathbf{w}}(\mathbf{w})=\int_0^{\infty} 2a\cdot p_z\left(a^2\right)\cdot\frac{1}{a^d}\cdot p_{\mathbf{x}}(\mathbf{w}/a)da \tag{91}$$

or:

$$ {}^4p_{\mathbf{w}}(\mathbf{w})=\int_0^{\infty} 2a\cdot\frac{1}{a^2}\cdot\frac{1}{a^d}\cdot\frac{1}{\left(2\pi\sigma^2\right)^{d/2}}\cdot e^{-\frac{\|\mathbf{w}\|^2}{2a^2\sigma^2}}da \tag{92}$$

The last equation can be put in the following form:

$$ {}^4p_{\mathbf{w}}(\mathbf{w})=\frac{2}{\left(2\pi\sigma^2\right)^{d/2}}\int_0^{\infty}\frac{1}{a^{d+1}}\cdot e^{-\frac{\|\mathbf{w}\|^2}{2a^2\sigma^2}}da \tag{93}$$

With the change of variable $a=1/t$ the pdf of $\mathbf{w}$ becomes:

$$ {}^4p_{\mathbf{w}}(\mathbf{w})=\frac{-2}{\left(2\pi\sigma^2\right)^{d/2}}\int_{\infty}^{0} t^{d+1}\cdot e^{-\frac{\|\mathbf{w}\|^2t^2}{2\sigma^2}}\frac{dt}{t^2} \tag{94}$$

For d=2, the bivariate pdf becomes:

$$ {}^4p_{\mathbf{w}}(w_1,w_2)=\frac{2}{\left(2\pi\sigma^2\right)}\int_0^{\infty} t\cdot e^{-\frac{\|\mathbf{w}\|^2t^2}{2\sigma^2}}dt \tag{95}$$

But:

$$ \frac{d}{dt}\left(e^{-\frac{\|\mathbf{w}\|^2t^2}{2\sigma^2}}\right)=-\frac{\|\mathbf{w}\|^2t}{\sigma^2}\cdot e^{-\frac{\|\mathbf{w}\|^2t^2}{2\sigma^2}} \tag{96}$$

Hence:

$$ t\cdot e^{-\frac{\|\mathbf{w}\|^2t^2}{2\sigma^2}}=-\frac{\sigma^2}{\|\mathbf{w}\|^2}\cdot\frac{d}{dt}\left(e^{-\frac{\|\mathbf{w}\|^2t^2}{2\sigma^2}}\right) \tag{97}$$

Substituting (97) in (95), this equation becomes:

$$ {}^4p_{\mathbf{w}}(w_1,w_2)=\frac{2}{\left(2\pi\sigma^2\right)}\int_0^{\infty}\left(-\frac{\sigma^2}{\|\mathbf{w}\|^2}\right)\cdot\frac{d}{dt}\left(e^{-\frac{\|\mathbf{w}\|^2t^2}{2\sigma^2}}\right)dt \tag{98}$$

or:

$$ {}^4p_{\mathbf{w}}(w_1,w_2)=-\frac{1}{\pi\|\mathbf{w}\|^2}\cdot e^{-\frac{\|\mathbf{w}\|^2t^2}{2\sigma^2}}\Big|_0^{\infty}=\frac{1}{\pi\|\mathbf{w}\|^2}=\frac{1}{\pi\left(w_1^2+w_2^2\right)}. \tag{99}$$

It results a third spherically-contoured bivariate pdf.
A last bivariate pdf for the wavelet coefficients was proposed in [17]:

$$ {}^5p_{\mathbf{w}}(w_1,w_2)=\frac{\gamma}{2\pi\left(w_1^2+w_2^2+\gamma^2\right)^{\frac{3}{2}}}. \tag{100}$$

4. Segmentation algorithms

In the following two segmentation algorithms will be presented. The first one uses a Euclidean distance and the second one uses the KL distance.

Digital image libraries are becoming more widely used as more visual information is put in digital form as well as on-line. To improve human access, however, there must be an effective and precise method for users to search, browse, and interact with these collections and to do so in a timely manner. As a result,

content-based image retrieval (CBIR) from un-annotated image databases has been a fast growing research area recently. A simple architecture of a typical CBIR system is presented in figure 3, where there are two major tasks.

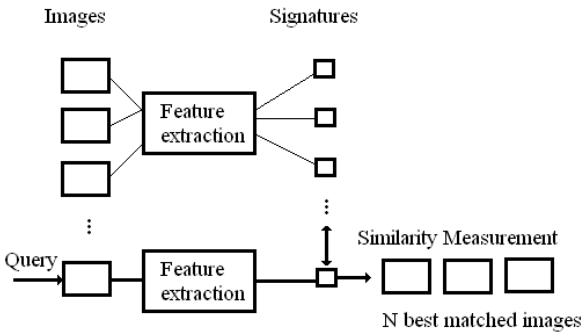

Figure 3. Typical architecture for a content-based image retrieval system.

The first one is feature extraction (FE), where a set of features, called image signatures, is generated to accurately represent the content of each image in the database. A signature is much smaller in size than the original image, typically on the order of hundreds of elements (rather than millions). The second task is similarity measurement (SM), where a distance between the query image and each image in the database using their signatures is computed so that the top "closest" images can be retrieved. Typically, the features used in CBIR systems are low-level image features such as color, texture, shape and layout. In this work, we focus on the use of texture information for image retrieval. Some of the most popular texture extraction methods for retrieval are based on filtering or wavelet-like approaches. Essentially, these methods measure energy (possibly weighted) at the output of filter banks as extracted features for texture discrimination. The basic assumption of these approaches is that the energy distribution in the frequency domain identifies a texture. Besides providing acceptable retrieval performance from large texture databases, those approaches are partly supported by physiological studies of the visual cortex. Furthermore, as wavelets are a core technology in the next generation of still image coding format, JPEG-2000, the choice of wavelet features enables the implementation of retrieval systems that can work directly in the compressed domain. Other possible transforms are wavelet packets, wavelet frames and Gabor wavelet transforms.
In [18] is proposed the following algorithm for image retrieval from data bases, which will be called algorithm 1:
Step 1. The Double Tree Complex Wavelet Transform (DTCWT) [19] of the image under processing is computed. This transform could be substituted with the HWT, because they have similar properties. The DTCWT has six subbands (each one with a different preferential orientation) and a variable number of resolutions. In [18] are used the first 4 resolution levels, obtaining an approximation sub-image and 24 detail sub-images.
Step 2. The features which will be used for segmentation are the mean and the standard deviation of the magnitude of the transform coefficients in each detail subband from each decomposition level. So, for a given image, a set of 48 features is obtained.
Step 3. To compare two images, one with feature vector **f**, and one with feature vector **g**, the distance metric used is:

$$d(\mathbf{f},\mathbf{g}) = \sum_{k=1}^{48} \frac{|f_k - g_k|}{\alpha_k} \tag{101}$$

where α_k is the standard deviation of feature *k* computed over the entire database.
This algorithm can be easy transformed into a segmentation algorithm (which will be called in the following algorithm 1') if the steps 2 and 3 are modified. In fact each retrieval algorithm has a correspondent segmentation algorithm. A retrieval algorithm aims to find similarities between two images belonging to the same data base and the purpose of a segmentation algorithm is to find similarities between two regions belonging to the same image. The step 2 must refer to the features of each block of pixels from the original image and the step 3 must compares these vector features and to allocate each block of pixels of the original image at a specified segment.

Generally, the SONAR images must be segmented in three types of regions: contours, textures and homogeneous regions. There are SONAR images which contain only textures. Those images must be segmented in three regions also. An example is presented in the following figure.

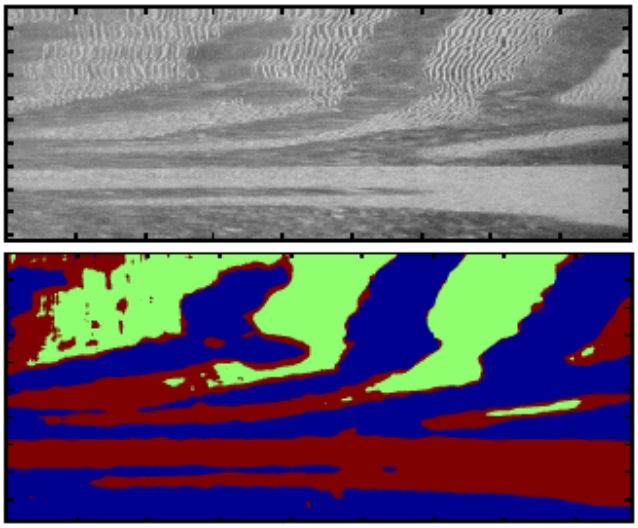

Figure 4. The segmentation of a SONAR image. Original image (up) and the segmentation result (bottom).

The example is taken from [23]. So, it is necessary to discriminate between different textures. Each region has a "center" with specific features. Computing the distance between the vector of features of the current pixel and the vector of features of each center and selecting the region at which corresponds the minimum distance, we can make the segmentation. Coming back to the previous example [18], the features which can be selected for segmentation in regions are: the preferential direction (indicated by the subband in which belongs the current wavelet coefficient), the decomposition level, the local mean of the wavelet coefficient (which indicates the level of brightness of the corresponding pixel) and the local standard deviation (which show if the considered pixel belongs to a region with rapid changes). The segmentation of SONAR images is made difficult by the existence of the speckle noise. A pretreatment phase in which is performed the despecklisation of the SONAR image is required before its segmentation. For the denoising, the wavelet transforms, which represent the subject of this rapport, are very useful, [20] and [21]. A SONAR images segmentation algorithm is proposed in the last reference. This algorithm can be enhanced if the information about the preferential directions of the wavelet coefficients is considered. Coming once again back to the reference [18] it must be said that the principal drawback of the algorithm 1 is the lack of a good statistical model for the features. If we assume that the features can be modeled as Gaussians with a common variance and just different means for the different classes then we end up with a squaring metric. However, such a metric has the problem that the difference between feature values of 100 and 101 is just as significant as that between values of 0.1 and 1.1. In [14] is presented a second algorithm for images retrieval from data bases based on the use of the KL distance. It will be called in the following algorithm 2.
The conventional scheme of multiscale texture analysis consist in extracting features from subband coefficients and use them as a signature associated with an appropriate distance to distinguish several texture classes. The drawback of this approach is the large volume of computation required when the number of features is high. Some others conventional approaches consist in representing detail subband coefficients by their probability density functions (PDFs). This is the approach preferred in the present rapport and this is the connection of the present section with the previous sections. Even that several probabilistic distances can be used, Do and Vetterli justified the use of Kullback-Leibler divergence (KLD) to have relevant results in retrieval application [22]. The same distance is used in [23].

Finding good similarity measures between images based on some feature set is a challenging task. On the one hand, the ultimate goal is to define similarity functions that match with human perception, but how humans judge the similarity between images is a topic of ongoing research. Perceptual studies identified texture dimensions by conducting experiments that asked observers to group textures according to perceived similarity. The detected perceptual criteria and rules for similarity judgment from this type of

subjective experiments can be used in building image retrieval system. On the other hand, many current retrieval systems take a simple approach by using typically norm-based distances (e.g., Euclidean distance) on the extracted feature set as a similarity function. The main premise behind these CBIR systems is that given a "good set" of features extracted from the images in the database (the ones that significantly capture the content of images) then for two images to be "similar" their extracted features have to be "close" to each other. Therefore, any reasonable similarity functions defined on the features space should perform well. Sometimes, weighting factors are necessary to normalize extracted features over the entire database to comparable ranges so that they have approximately the same influence on the overall distance. Note that this "global" normalization process is different with the one often used in classification problems where the normalized factors are computed using a training set of feature vectors from each class. Furthermore, the commonly used inverse variance weighted Euclidean distance as in CBIR is questionable in the case of a feature component that has small global variance, thus leading to a large weight in the overall distance. By contrast, it can be argued that a small variation component should have little discrimination power and should thus carry a small weight in the overall distance.

In this work we consider jointly the problems of FE and SM in texture retrieval using a statistical approach. Our point is that, given only a low-level representation, statistical modeling provides a natural mean to formulate the retrieval problem, as is typically done in pattern recognition. Considering the two related retrieval tasks FE and SM as estimation and detection problems, respectively, provides us with a justified way of defining similarity functions on the feature space. The implication of this approach is twofold. First, it provides a confidence on the optimality of the defined similarity function under some explicit assumptions. Secondly, this approach provides a common ground for many existing similarity functions by simply modifying the underlying assumptions. Statistical modeling has been used in CBIR systems before. Perhaps the most well-known examples are the use of histograms to capture the distribution of image features such as color. The generalized Gaussian density functions were already employed to represent texture images in the wavelet domain. The model parameters are estimated using a method of moment matching, and the similarity function is again defined as weighted Euclidean distances on extracted model parameters.

Recently was taken a similar approach by introducing a probabilistic formulation of the CBIR problem as a common ground for several currently used similarity functions. As an important case of CBIR, it is demonstrated in [22] the application of the statistical framework in the wavelet-based texture retrieval problem. The statistical approach fits nicely into this case, since a texture image is often regarded as a realization of an underlying stochastic process.

The problem of searching for the top N images similar to a given query image from a database of total M images ($N \ll M$) can be formulated as a multiple hypotheses problem. The query image I_q is represented by its data set $\mathbf{x}=\left(x_1, x_2, ..., x_L\right)$, which is typically obtained after a pre-processing stage. Each candidate image in the database I_i: i=1, 2, …,M is assigned with a hypothesis $\mathcal{H}_i$. The goal is to select among the M possible hypotheses the N best ones (with a ranking order) that describe the data $\mathbf{x}$ from the query image.

To select the N top matches from those M hypotheses we can use the multiple hypotheses testing argument recursively. That is, we first choose the best one among the M possible hypotheses $\left\{\mathcal{H}_1, \mathcal{H}_2, ..., \mathcal{H}_M\right\}$, and then we choose the next best one among the remaining M-1 hypotheses, and keep doing so for N times. Under the common assumption that all prior probabilities of the hypotheses are equal, it can be shown that, for each recursive step the optimum rule (with the minimum probability of error criterion) is to choose the hypothesis with the highest likelihood among the possible ones. Thus for CBIR, it is optimal to select N hypotheses with highest likelihood, i.e. $\mathcal{H}_{k_1}, \mathcal{H}_{k_2}, ..., \mathcal{H}_{k_N}$ where

$$p\left(\mathbf{x}\middle|\mathcal{H}_{k_1}\right) \geq p\left(\mathbf{x}\middle|\mathcal{H}_{k_2}\right) \geq ... \geq p\left(\mathbf{x}\middle|\mathcal{H}_{k_N}\right) \geq p\left(\mathbf{x}\middle|\mathcal{H}_i\right) \qquad i \neq k_j \ \ (j=1, 2, ..., N). \tag{102}$$

This is referred to as the maximum likelihood (ML) selection rule. The problem with (102) is that it requires M computational steps with a typically large data set $\mathbf{x}$. This turns out to be impractical in CBIR applications since this operation has to be done on-line in the interactive mode. Therefore, we need to find an approximation with much less computational cost.

In the parametric approach, the conditional probability density $p\left(X\left|\mathcal{H}_i\right.\right)$ is modeled by a member of a family of pdfs, denoted by $p\left(X;\boldsymbol{\theta}_i\right)$ where $\boldsymbol{\theta}_i$ is a set of model parameters. With this setting, the extracted features for the image I_i are the estimated model parameter $\hat{\boldsymbol{\theta}}_i$, which is computed in the FE step. We denote the space of model parameters as $\boldsymbol{\Theta}$. Consider the query data $\mathbf{x}=\left(x_1,x_2,...,x_L\right)$ as an independent and identically distributed (i.i.d.) sequence from the model $p\left(X;\boldsymbol{\theta}_q\right)$ of the query image. Then for large L, using the weak law of large number, the ML selection rule (102) is equivalent to maximizing

$$\frac{1}{L}log\ p\left(\mathbf{x};\boldsymbol{\theta}_i\right)=\frac{1}{L}\sum_{j=1}^{L}log\ p\left(x_j;\boldsymbol{\theta}_i\right)\overset{L\to\infty}{\to}E_{\boldsymbol{\theta}_q}\left\{log\ p\left(X;\boldsymbol{\theta}_i\right)\right\}= \\ =\int_{-\infty}^{\infty}p\left(x;\boldsymbol{\theta}_q\right)log\ p\left(x;\boldsymbol{\theta}_i\right)dx. \tag{103}$$

This can be seen as equivalent to minimizing the Kullback–Leibler distance or the relative entropy between the two pdfs $p\left(x;\boldsymbol{\theta}_q\right)$ and $p\left(x;\boldsymbol{\theta}_i\right)$

$$D\left(p\left(X;\boldsymbol{\theta}_q\right)\middle\|p\left(X;\boldsymbol{\theta}_q\right)\right)=\int_{-\infty}^{\infty}p\left(x;\boldsymbol{\theta}_q\right)log\frac{p\left(x;\boldsymbol{\theta}_q\right)}{p\left(x;\boldsymbol{\theta}_i\right)}dx. \tag{104}$$

Under the same asymptotic condition (L is large), if the FE step uses a consistent estimator, which ensures the estimated parameter $\hat{\boldsymbol{\theta}}$ converges to the true parameter $\boldsymbol{\theta}$, then the distance (104) can be computed using the estimated model parameters $\hat{\boldsymbol{\theta}}_q$ and $\hat{\boldsymbol{\theta}}_i$. For such consistent estimator, we could employ the ML estimator, which means that for the query image, it computes

$$\hat{\boldsymbol{\theta}}_q=\underset{\boldsymbol{\theta}\in\boldsymbol{\Theta}}{arg\ max}\ log\ p\left(\mathbf{x};\boldsymbol{\theta}\right). \tag{105}$$

In summary, by combining FE and SM into a joint modeling and classification scheme, the optimum ML selection rule can be asymptotically realized (as the data sets for each image become large). So the algorithm 2 has the following structure:

Step 1. The WT of the image which represents the query is computed.

Step 2. FE. The parameters of the model (which is in the case of [22] the GG family and in the case of [14] the Asymmetric Generalized Gaussian (AGG) family) are identified in each subband at each decomposition level. This way, the pdfs $p\left(\mathbf{x};\boldsymbol{\theta}\right)$ are constructed.

Step 3. SM. The KLD between the pdfs obtained as a result of the previous step and all the corresponding pdfs of the other images from the data base are computed and the image with the minimum KLD is retrieved.

This algorithm can be modified to obtain the algorithm 2' designed for segmentation if the image to be processed is divided into non overlapping blocks. Next, each of these blocks is regarded as a query and the regions which represent the result of segmentation are regarded as the elements of the data base. For each block is applied the algorithm 2, retrieving the region at which it belongs. Finally, by the concatenation of all the blocks corresponding to each region the segmentation is obtained.

For the segmentation of SONAR images we propose to use the algorithm 2' associated with the HWT (or with the HWPT) and with the models given in equations (87), (99) or (100) or in table 1.3.1.1. Their major advantage is the fact that they have only one parameter, the local standard deviation.

5. Conclusions

The aim of this rapport is to propose a new segmentation algorithm for SONAR images. The advantages of this algorithm are:

- it is fast, because the WTs are some of the faster transforms used in signal and image processing,
- it takes better into account the directions of the different objects which belong to a given SONAR image because it uses the HWT or the HWPT which are transforms with higher directional selectivity,
- it is precise, because it uses a good model for the wavelet coefficients, which takes into account their interscale dependence.

With minor modifications the algorithm proposed can be used for image retrieval from data bases. Before the application of the segmentation algorithm the SONAR image must be denoised. Because the two

procedures, the denoising and the segmentation use similar ingredients (the HWT, the same statistical model of the wavelet coefficients) the computation required by the segmentation algorithm can be simplified, some operations being already made by the denoising algorithm.

References

[1] Corina Botoca, Adaptive Systems with Neural Networks, advised by professor Nafornita and presented in 1998, http://hermes.etc.upt.ro/cercetare/sp.html

[2] Sorin Moga (France) Apprendre par imitation: une nouvelle voie d'apprentissage pour les robots autonomes, advised by professor Philippe Gaussier from ENSEA Cergy-Pontoise, France and professor Ioan Nafornita.

[3] Ileana Popescu (Greece), Neural network applications for radio-coverage studies in mobile communication systems, advised by professor Philip Constantinou from NTUA Greece and by professor Ioan Nafornita.

[4] Oltean M., Boucher J.-M., Isar A. Diversity-Enhanced Wavelet Domain Applied to ECG Signals Denoising, Speech and Signal Processing, ICASSP 2006 Volume 2, 14-19 May 2006 Page(s):II-1196 - II-1199, ISBN 1-4244-0469-X,

[5] Stolojescu Cristina, Estimation de contexte de bruit par filtrage en ondelettes, Stage Erasmus effectue a LTSI, Laboratoire de Traitement du Signal et de l'Image, de l'Université de Rennes 1, France, Professor coordinator, Guy Carrault,

[6] Isar D., Isar A., Quinquis A. Multi-scale MAP Denoising of SAR and SAS Images, Sea Technology Magazine, February 2007, 46-48, ISSN 0093-3651,

[7] Kovaci M., Balta H., Isar A., Oltean M., Salagean M., How could be better defined an effective CINR for multi-carrier modulation user in order to effectively determine the link error performance obtained ? October 2007,

[8] Karaoui Imen**,** Segmentation par méthodes markoviennes et variationnelles des images texturées: application à la caractérisation sonar des fonds marins, adviser Prof. Boucher Jean-Marc, ENST-B 2007.

[9] A. M. Atto, D. Pastor, Central Limit Theorems for Wavelet Packet Decompositions of Stationary Random Processes, submitted to IEEE Transactions on Signal Processing, Accepted for future publication.

[10] Ioana Adam, Corina Nafornita, Jean-Marc Boucher, Alexandru Isar," A New Implementation of the Hyperanalytic Wavelet Transform", International Symposium on Signal, Circuits and Systems, ISSCS 2007, Iasi, Romania, 12-13 July 2007.

[11] Ioana Firoiu, Dorina Isar, Jean-Marc Boucher, Alexandru Isar, Hyperanalytic Wavelet Packets, Proc. WISP 2009, 6th IEEE International Symposium on Intelligent Signal Processing , 26–28 August, 2009 Budapest, Hungary, 67-72, ISBN: 978-1-4244-5058-9

[12] L. Sendur and I. W. Selesnick, "Bivariate shrinkage functions for wavelet-based denoising exploiting interscale dependency", *IEEE Trans. on Signal Processing*, 50(11), '02, 2744-2756.

[13] Stephan Mallat, A wavelet tour of signal processing, 2nd Edition, *Academic Press*, New York, 1999.

[14] Nour-Eddine LASMAR, Youssef STITOU, Yannick BERTHOUMIEU, Multiscale Skewed Heavy Tailed Model For Texture Analysis, 2009 IEEE International Conference on Image Processing, Cairo, Egypt, November 2009,

[15] Ivan W. Selesnick, The Estimation of Laplace Random Vector in AWGN and the Generalized Incomplete Gamma Function, IEEE Trans. on Signal Processing, 56(8):3482-3496, August 2008.

[16] J. Portilla, V. Strela, M. J. Wainwright, and E. P. Simoncelli, "Image denoising using Gaussian scale mixtures in the wavelet domain," *IEEE Transactions on Image Processing*, vol. 12, no. 11, pp. 1338–1351, Nov 2003.

[17] A. Achim and E. E. Kuruoglu, "Image Denoising Using Bivariate α-Stable Distributions in the Complex Wavelet Domain", *IEEE Sig. Proc. Let.*, 12(1), '05, 17-20,

[18] Peter de Rivaz and Nick Kingsbury, Complex Wavelet Features for Fast Texture Image Retrieval, ICIP (1) 1999: 109-113,

[19] N G Kingsbury, "Shift invariant properties of the Dual-Tree Complex Wavelet Transform", *Proc. IEEE Conf. on Acoustics, Speech and Signal Processing*, Phoenix, AZ, paper SPTM 3.6, March 16-19, 1999.

[20] Firoiu I., Nafornita C., Boucher J. –M., Isar A., Image Denoising Using a New Implementation of the Hyperanalytic Wavelet Transform, IEEE Transactions on Instrumentation and Measurements, vol. 58, Issue 8, August 2009, pp. 2410-2416, Digital Object Identifier 10.1109/TIM.2009.2016375, ISSN: 0018-9456,

[21] Alexandru Isar, Sorin Moga, Dorina Isar, A New Denoising System for SONAR Images, EURASIP Journal on Image and Video Processing, Hindawi Publishing Corporation, Volume 2009 (2009), Article ID 173841, doi: 10.1155/2009/173841,
[22] M.N. Do and M. Vetterli, "Wavelet-based texture retrieval using generalized Gaussian density and Kullback-Leibler distance," *IEEE Trans. Image Processing*, vol. 11, 2002, pp. 146-158.
[23] Karoui Imen, Ronan Fablet, Jean-Marc Boucher and Jean-Marie Augustin, Statistical discrimination of seabed textures in sonar images using co-occurrence statistics, Proceedings of the IEEE international conference Oceans 2005.